DIRECT TRIPLET STATE EXCITATION OF INDOLE DERIVATIVES: NOVEL

APPLICATIONS OF PHOSPHORESCENCE

By

JOSE LUIS CHAVEZ

Bachelor of Science, 2015
University of Texas at Arlington
Arlington, Texas

Master of Arts, 2018
Texas Christian University
Fort Worth, Texas

Submitted to the Graduate Faculty of the
College of Science and Engineering
Texas Christian University
in partial fulfillment of the requirements
for the degree of

Doctor of Philosophy

TCU

August 2022

APPROVAL

DIRECT TRIPLET STATE EXCITATION OF INDOLE DERIVATIVES: NOVEL

APPLICATIONS OF PHOSPHORESCENCE

by

Jose Luis Chavez

Dissertation approved:

_____

Dr. Zygmunt Gryczynski, Major Professor and W.A. "Tex" Moncrief Jr. Chair of
Physics

_____

Dr. Yuri M. Strzhemechny, Department Chair and Associate Professor of Physics

_____

Dr. Anton V. Naumov, Associate Professor of Physics

_____

Dr. Hana M. Dobrovolny, Associate Professor of Physics

_____

For the College

ACKNOWLEDGMENTS

I would like to thank my advisor Dr. Zygmunt "Karol" Gryczynski, for allowing me to have the opportunity to research time-resolved fluorescence spectroscopy. He has taught me to think outside the box, ask questions, and never stop being creative when solving problems.

Thank you, Dr. Ignacy Gryczynski, for opening the doorway to the phosphorescence realm. You taught me how to write papers and how to deal with reviewers.

I also like to thank my committee members, Dr. Strzhemechny, Dr. Naumov, and Dr. Dobrovolny, for their valuable input and for teaching me Graduate Quantum Mechanics, Solid State Physics, and Non-linear Dynamics.

To my lab members Zhangatay Nurekeyev, Dr. Joseph Kimball, Luca Ceresa, and Emma Kitchner, thank you so much for being fabulous lab partners and for taking in my "dad jokes."

Thank you, Carol Brooks, for providing me with coffee and tea during this period of writing this thesis.

Thank you, Arek Matwijczuk, for being an incredible mentor and keeping me active physically and mentally!

Lastly, I would like to thank my mother and father, Maria and Jose Chavez, for giving me all their love and support. Lastly, one huge thanks to my brother and sister, David and Victoria, for being the best siblings I could ever ask for.

TABLE OF CONTENTS

LIST OF FIGURES

vii

LIST OF TABLES

LIST OF ABBREVIATIONS

Chapter 1 Introduction

IC: Internal Conversion

S_i: Singlet excited state of the ith level

T_i: Triplet excited state of the ith level

ISC: Intersystem Crossing

Γ: Fluorescence radiative rate

Γ_p: Phosphorescence radiative rate

k_{nr}: Non-radiative rate (fluorescence)

k_{isc}: Intersystem crossing rate

R6G: Rhodamine 6G

τ: Lifetime

2PI: 2-Phenylindole

5-BrI: 5-Bromoindole

M_A: Absorption transition moment

N_A: Avogadro number

TRP: Tryptophan

HSA: Human serum albumin

RTP: Room temperature phosphorescence

Chapter 2 Methodology

HPLC: High-Performance Liquid Chromatography

DI: Deionized

UV: Ultraviolet

s: Seconds

ms: Milliseconds

GmbH: Gesellschaft mit beschränkter Haftung (company with limited liability)

PMT: Photomultiplier tube

MCP: Microchannel plate

$< \tau >_{int}$ or $\bar{\tau}$: Intensity average lifetime

$< \tau >_{amp}$ or $< \tau >$: Amplitude average lifetime

α_i: Amplitude of ith component

G-factor: Geometric factor

H: Horizontal

V: Vertical

2AP: 2-Aminopurine

BBO: 2,5-bis-(4-biphenylyl)-oxazol

C153: Coumarin 153

Ru: Ruthenium bipyridyl, $[Ru(bpy)_3]^{2+}$

amu: Atomic mass unit

Chapter 3 Results

A.U.: Arbitrary units

nm: nanometer

QS: Quinine sulfate

H_2SO_4: Sulfuric acid

QY: Quantum yield

ns: nanosecond

PMMA: Poly (methyl Methacrylate))

Chapter 1 Introduction

Photophysics is the study of the interaction of light and matter. When this interaction occurs, molecules (components of matter) can absorb light and consequently release a photon of different energy in a process called emission. The emission of a photon, some time duration after the absorption of a photon, is called photoluminescence. Photoluminescence can be separated into two processes, fluorescence, and phosphorescence.

1.1 Fluorescence

A simple diagram called the Jablonski diagram, as shown in Figure 1, schematically illustrates the processes involved in the interaction of light and molecules.
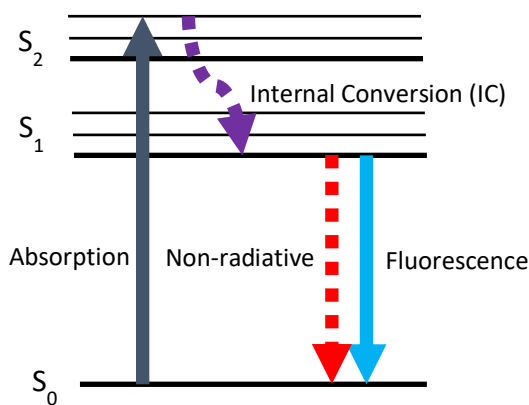
Figure 1. Jablonski diagram where the solid lines involve the process of a photon (radiative) while dashed lines (non-radiative) do not.

Horizontal lines (S_0, S_1, ...) correspond to the allowed energetic states of the molecule. The energy of the absorbed photon (process indicated by a gray vertical arrow in Figure 1) must be equal to the energy difference between the higher energy state called the excited state (S_i) and the energy of the ground state (S_0). As a consequence of the absorption of a photon of given energy, the

molecule transits from the ground state to an excited state ($S_0 \rightarrow S_i$). The photon absorption is a result of the interaction of electronic orbitals of a molecule with the electromagnetic field of the photon, a process that happens in 10^{-15} s. Once the molecule absorbs light, it is then excited to the corresponding allowed singlet states (S_i). This is typically an unstable state without constant energy input to maintain the high energy level, and the molecule quickly relaxes (10^{-14} to 10^{-11} s) to the first allowed singlet state (S_1) through a process called internal conversion (IC). During this process, the excess energy is dissipated in the form of heat through non-radiative transitions (shown as the purple dashed line). The first excited state (S_1) is stable, and the molecule can stay in this state for a longer time before deactivating to the ground state (depending on the conditions, 10^{-10} s to 10^{-7} s). The first excited state (S_1) is what is considered a metastable state. The transition from the first excited state can be a non-radiative process through multiple vibrational states where the energy is lost in the form of heat (dashed red line). Or it can be a single step transition to one of the lower vibrational states of the ground state with the excess of excitation energy realized in the form of a photon (emission). Molecules that absorb and emit light are frequently called chromophores or fluorophores.

1.2 Phosphorescence

After absorption, when the fluorophore is in the first singlet excited state, S_1, an alternative deactivation process can occur. When highly perturbed, the excited molecule can transit to a state called the triplet state T_1 (Figure 2). This transition (yellow dashed line) is called intersystem crossing (ISC) and is quantum mechanically forbidden due to the violation of the conservation of angular momentum. Subsequently, the fluorophore will relax to the lowest triplet excited state, and the excess energy is released in the form of heat. The transition from the first triplet state T_1 to the ground state S_0 is also forbidden, again violating conservation of angular momentum.

Consequently, the molecule can stay in this state for longer (10^{-6} s or more). The transition to the ground state can be in a non-radiative way or in a single step with the emission of a photon, a process called phosphorescence.
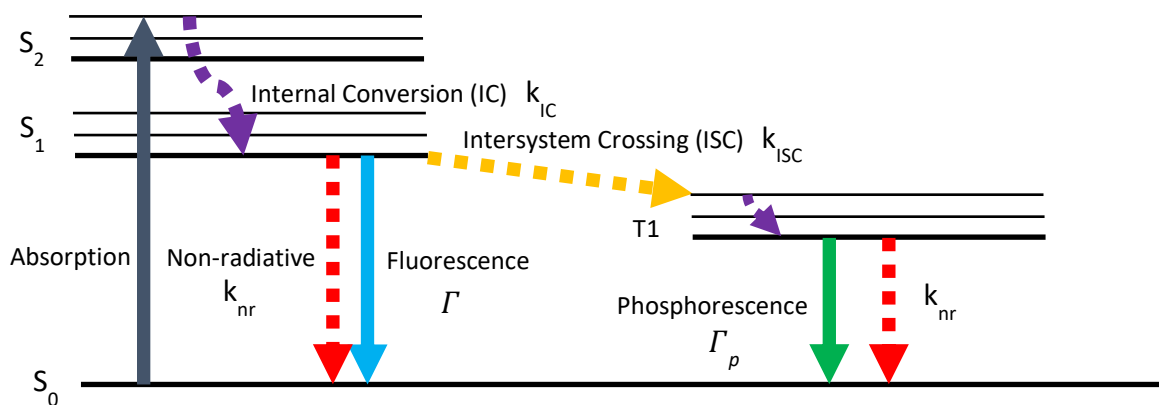
Figure 2. Jablonski diagram with the extension of the triplet state (T_1). Each process is labeled with a rate k_i where 'i' being nr non-radiative, IC internal conversion, and ISC intersystem crossing. Γ is the fluorescence radiative rate and Γ_p is the phosphorescence radiative rate. The solid lines involve the process of a photon (radiative) while dashed lines (non-radiative) do not.

Each of these rates labeled with 'k' describes the probability of events per unit of time. Beginning with k_{IC} is the rate of internal conversion. Internal conversion is a non-radiative transition between two electronic states of the same spin multiplicity. The non-radiative rate is the photon energy dispersed as vibrations or heat. Fluorescence radiative rate, Γ is the emissive rate from the first excited singlet state to the singlet ground state. Intersystem crossing rate k_{ISC} is the non-radiative transition between two isoenergetic vibrational levels belonging to electronic states of different multiplicities. Lastly, Γ_p is the emissive rate from the first excited triplet state to the singlet ground state.

1.3 Absorption Spectrum

The electromagnetic field of incoming light interacts with the electronic orbitals of the molecule and can promote the transition of the molecule from the ground state to a higher, excited energy state. The probability for the photon to interact with the molecule is generally proportional to the density distribution of allowed excited states. Consequently, the energy of the light (photon) being absorbed by the molecule leads to light attenuation. The light attenuation process is called absorption. The primary factors responsible for light absorption by molecules are:

1. The energy of the incident photon must correspond to the energy difference of two given states, which we can represent as $hv = S_i - S_0$

2. The strength of the absorption oscillator is called the dipole transition moment. The quantity expresses the probability of absorption or emission of electromagnetic radiation in transitions between energy levels of a molecule. This is manifested by the absorption cross-section, σ, of a given molecule (fluorophore). This parameter reflects the probability of a photon passing in the molecule's proximity to be absorbed. In chemistry, it is referred to as the extinction coefficient, ε.

3. The concentration of the molecules.

4. The intensity of the excitation light source dictates the number of molecules being excited.

5. The relative orientation between the vector of polarization of the excitation light and the molecular dipole transition moment. Transition moments have well-defined directions in a molecular framework. Thus, the probability of interacting with the incoming light depends on $cos^2 \alpha$, where α is the angle between the transition moment direction and the vector of light polarization.

The concentration of molecules in a solution, C, is typically given in moles per liter [mol/L]. The number of molecules per cubic centimeter [number of molecules/cm^3] can be calculated using Avogadro's number (N_A - 6.0225×10^{23} mol^{-1}) and the conversion factor from [mol/L] as $C*N_A$ /1000. The absorption cross-section is wavelength (photon energy) dependent, and at any given wavelength, λ, is represented by $\sigma(\lambda)$, and its unit is [cm^2/mol]. The absorption cross-section reflects the probability that a photon of a given wavelength (energy) will be absorbed as it passes the fluorophore's proximity. We must remember that a typical molecule is much smaller than the wavelength of light and the incoming/passing electromagnetic radiation produces a local field perturbation. A fluorophore in such a field has a certain probability of absorbing the energy that depends on the density distribution of allowed states of the molecule. As the light of suitable energy (wavelength) travels through the solution of fluorophores, it can be absorbed by the individual fluorophore. The number of absorbed photons will depend on the number of fluorophores in the light's path. In typical conditions, one fluorophore absorbs one photon, and the number of absorbed photons will be proportional to the number of available chromophores present in the light's path, Δl. Thus, the change in intensity of light, ΔI, as it travels through the solution is

$$\Delta I = I_0 n \Delta l \sigma, \tag{1}$$

where I_0 is the intensity of the incoming light wave (number of photons per surface unit per second), Δl is the path length, and n is the number of fluorophores per unit of volume. The intensity of the transmitted light, I, for a sample of thickness, l, can be expressed by

$$I = I_0 e^{-\sigma n l}. \tag{2}$$

Equation (2) is known as the Beer-Lambert law. It is useful to rewrite the Beer-Lambert law as a function of wavelength because the absorption cross-section is wavelength-dependent

$$I(\lambda) = I_0(\lambda) e^{-\sigma(\lambda) n l}. \tag{3}$$

Absorption is represented by the exponential factor $\sigma(\lambda)nl$. The value can be calculated using log base 10 or log base e, decadic or Napierian, respectively. The extinction coefficient $\varepsilon(\lambda)$ is more frequently used in photochemistry and photobiology. The molar extinction coefficient measures how strongly a chemical species absorbs at a particular wavelength with units m^2/mol, but is usually expressed in $m^{-1}cm^{-1}$. The units for the molar extinction coefficient are [L mol^{-1} cm^{-1}], although the units used may vary by the field (i.e., [m^2 mol^{-1}]). The decadic molar extinction coefficient, $\varepsilon(\lambda)$, is used in this text. It relates to the absorption cross-section as

$$\sigma(\lambda) = \frac{2.303\ \varepsilon(\lambda)}{N_A} = 3.823 * 10^{-21}\ \varepsilon(\lambda). \tag{4}$$

Thus, as a general rule, the natural logarithm will also be used when the absorption cross-section σ is used. When the extinction coefficient ε is used, the logarithm will be taken with base 10. The Beer-Lambert law then becomes

$$I(\lambda) = I_0(\lambda)10^{-\varepsilon(\lambda)Cl}. \tag{5}$$

Where C is the molar concentration of the molecule and the exponent's base is ten instead of e. One must be aware of this, as all texts do not adopt this convention. The absorbance "Abs," or sometimes referred to as the optical density (OD), is defined as

$$Abs(\lambda) = \varepsilon(\lambda)Cl. \tag{6}$$

Absorbance is a unit-less quantity, which is the argument of the exponent in the Beer-Lambert law.

1.4 Transition Dipole Moment

A transition between energy levels requires a quantized well-defined amount of photon energy. But there are additional restrictions for a transition to take place. Those restrictions come from the nature of the interaction between electromagnetic radiation and matter, which are summarized by

the selection rules. Light is consisting of orthogonally oscillating electric and magnetic fields. The electric field interacts with the electric charges and is the primary factor responsible for electronic transitions. We can obtain the energy of an interaction between the electric field and a system of charged particles by calculating the scalar product of the electric field vector $\vec{\varepsilon}$ and the dipole moment vector $\vec{\mu}$ of the system of charges.

$$E = -\vec{\mu} \cdot \vec{\varepsilon}. \tag{7}$$

The dipole moment vector μ is defined as the summation of the product of each charged particle q_i and its corresponding position vector r_i,

$$\mu = \sum_i q_i \cdot r_i. \tag{8}$$

The expectation value for the interaction energy E can be calculated as

$$< E > = \int \psi_n^* (-\hat{\mu}.\hat{\varepsilon}) \psi_n d\rho. \tag{9}$$

Where $\int d\rho$ refers to the integral over all coordinates. Operator $\hat{\mu}$ and $\hat{\varepsilon}$ are vectors with the magnitude of the classical quantities μ and ε.

For visible light that has a wavelength much longer than the length of a molecule, the magnitude of the electric field can be seen as a constant across the length of the molecule. Therefore, the component ε can be taken out of the integral and give the expected value for the permanent dipole moment of the molecules in state n,

$$< \mu > = \int \psi_n^* (-\hat{\mu}) \psi_n d\tau. \tag{10}$$

Thus, the energy of the interaction depends on the dipole moment of the system that represents charge distribution.

We are particularly interested in the transition between states and the corresponding strength of the interaction's energy. Therefore, we use the transition dipole moment as a substitute for the dipole moment. The transition dipole moment integral is conceptually similar to the integral of the dipole moment. The difference lies in the two wave functions of distinguished states, the initial (ψ_i) and final (ψ_f) states,

$$< \mu_T >= \int \psi_f^* (-\hat{\mu}) \psi_i d\tau = \mu_T. \tag{11}$$

In the case of $< \mu_T > = 0$, the transition is said to be forbidden. If $< \mu_T > > 0$, the transition is allowed.

A molecule typically has multiple absorption transition moments corresponding to transitions to different excited electronic states of the molecule (different absorption bands). Upon interacting with light, a molecule will preferentially absorb light with a polarization vector of the electric field parallel to the direction of the chromophore transition moment.

The absorption spectrum represents the probability distribution for photons of given energies to be absorbed by the molecule. An example of an absorption spectrum is shown below for rhodamine 6G (R6G), Figure 3.
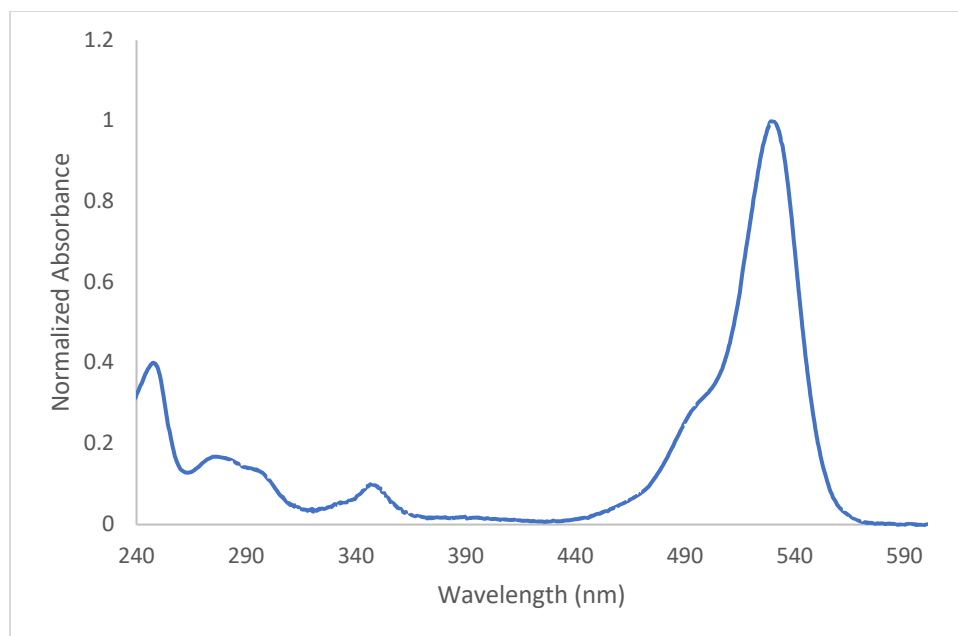
Figure 3. The absorption spectra of rhodamine 6G.

1.5 Emission Spectra

Visible emission typically happens from the first excited state (S_1 to S_0), and the molecule has a single transition moment associated with emission. An excited molecule can only emit photons with an electric field vector parallel to the molecule transition moment. The emission spectrum is the wavelength distribution of the emitted energy (number of emitted photons at a given wavelength), measured at a single constant excitation wavelength. The recorded emission spectrum represents the photon emission rate or power emitted at a given wavelength. Emission spectra are the characteristic of any fluorophore and generally depend on the chemical structure of the fluorophore and the solvent in which it is dissolved. An example of R6G's emission spectrum is shown in Figure 4.
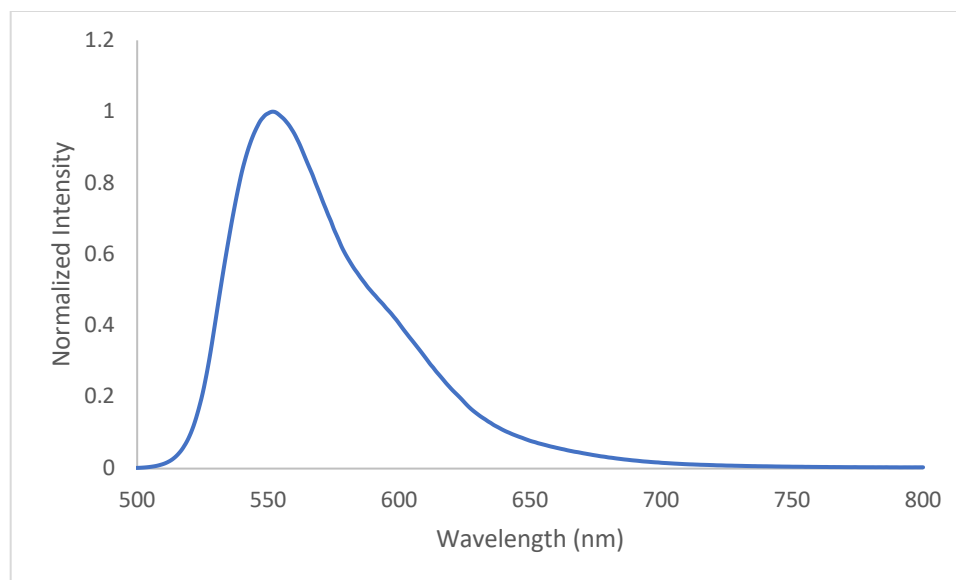
Figure 4. An example of emission spectra of rhodamine 6G (R6G).

1.6 Stokes shift

When absorbing a photon, the molecule transits to the high vibrational state of one of the allowed electronic excited states. The molecule rapidly relaxes to the lowest excited state after interactions with the solvent/enviornment, and the excess energy is quickly lost via transitions through vibrational and rotational states as heat. As the result of the radiative transition from the lowest excited state to a ground state, the molecule emits a photon of well-defined but lower energy as compared to the absorbed photon. Consequently, the emission spectrum will be shifted to a longer wavelength, this phenomenon was first reported by Stokes. The difference between the maximum absorbance and maximum emission is called Stokes' shift, as shown in Figure 5.
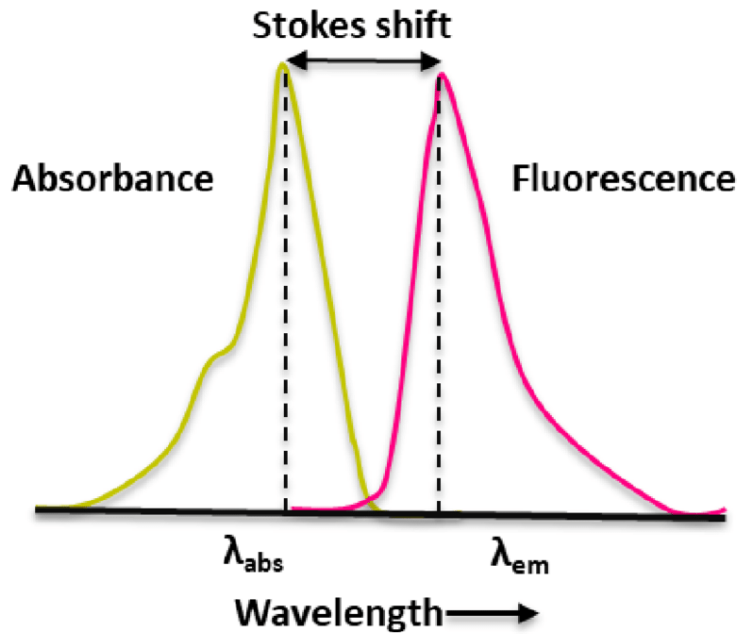
Figure 5. Diagram of absorption spectra (lime) as well as emission spectra of fluorescence (red). The stoke shift is shown between the dotted lines.

1.7 Polarization

Unpolarized (isotropic) light I_0 of the type, such as an incandescent or arc lamp, has equal amplitudes of the electric vector orthogonal to the direction of light propagation. A polarizer is an optical element that only allows the light of a particular polarization plane to be transmitted. Shown below in Figure 6 are two polarizers and the transmission (I) of light through each polarizer.
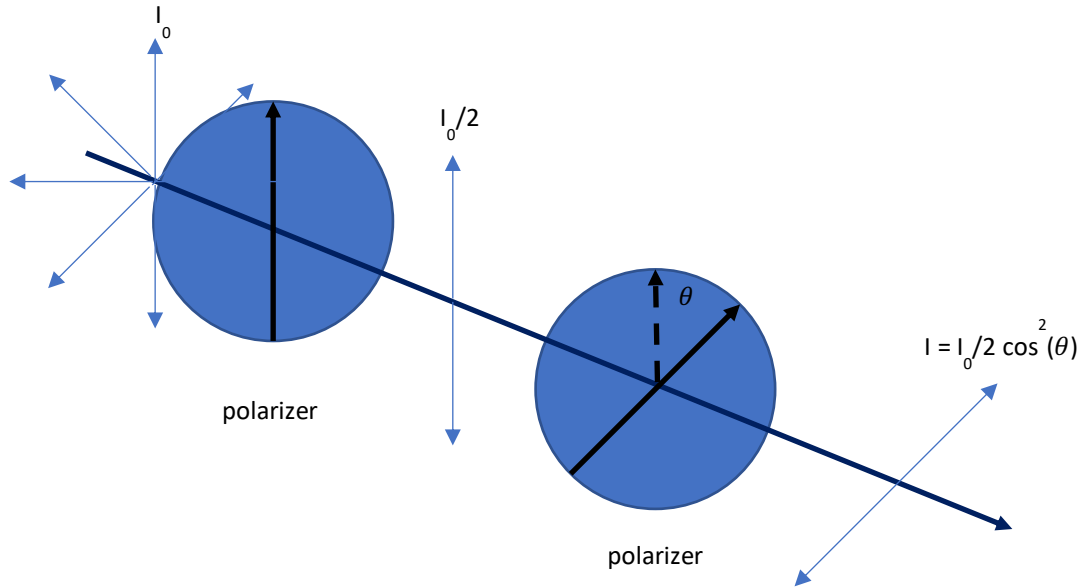
Figure 6. The incident light, I_0, is unpolarized. Only vertically polarized light passes through the first polarizer, $\theta = 0$. Transmission through the second polarizer is proportional to $cos^2(\theta)$. The angle θ is between the principal axis of the first polarizer (dotted on the second polarizer) and the second principal axis (solid black line).

As the unpolarized light passes through the first polarizer with an angle of 0 degrees with respect to the verticle axis, as shown in Figure 6, only vertically polarized light transmits, and the intensity, I_0, drops by half. If the second polarizer is rotated by some angle theta with respect to the first polarizer, the intensity is then described by

$$I = I_0 cos^2(\theta), \tag{12}$$

where I_0 is the intensity of light incoming to the polarizer. The maximum transmitted light through the second polarizer is when $\theta = 0$ and intensity I decreases as angle θ increases, and for $\theta = 90$ degrees, there is no light transmitted. Equation 12 is known as the Malus' Law.

1.8 Photoselection and Anisotropy

For linear transition moments, absorption of light by a molecule depends on the relative orientation of its transition moment (dashed line, Figure 7) in relation to the direction of light polarization (solid line, Figure 7).

$$\text{No absorption} \qquad \text{Absorption} \qquad \text{Absorption} \propto cos^2(\theta)$$

$$\theta = 90^0 \qquad\qquad \theta = 0^0$$
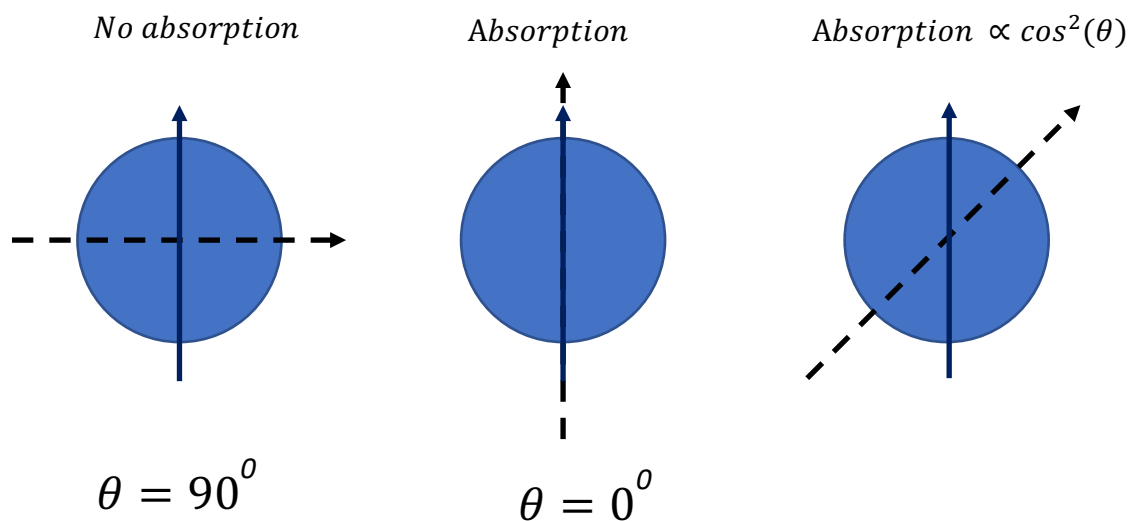
Figure 7. Interaction of polarized light (solid black line) with the absorption transition moment (dashed line) of a fluorophore. (Left) shows no absorption of the fluorophore if the angle θ between the polarized light and transition moment are orthogonal to each other. (Middle) shows the maximum probability of absorption if the angle theta is zero or collinear. (Right) shows the probability of absorption is cosine squared of the angle theta.

The probability of excitation of a chromophore is proportional to the cosine squared of the angle theta between the polarization of light and the transition moment of the molecule. The probability is maximum when the molecule's transition moment is parallel to the light polarization vector ($\theta = 0$ degrees). The probability is zero when the molecule's transition moment is orthogonal to

the light polarization ($\theta = 90$ degrees). For any other orientation of the transition moment in relation to the light polarization (angle θ between the polarization of light (solid line) and tranisition moment (dashed line), figure 7 right), the probability of absorption is proportional to $\cos^2 \theta$. The absorption process of polarized light results in a non-isotropic distribution of excited molecules called photoselection.

Anisotropy is a consequence of the linear transition moments associated with absorption and emission processes [27]. All organic molecules have a well-defined fixed linear transition moments within their molecular structure. The probability for a given molecule to absorb a photon is proportional to $cos^2(\theta)$ where θ is the angle formed between the direction of the molecule's transition moment and the plane of polarization for the photon. Excited molecules with polarized light will be selected to form a non-isotropic distribution of excited molecules. After the excited molecules emit, the emission will be non-isotropic. Polarization of the emitted light will depend on the relative orientation of the absorption transition moment and the emission transition moment in the moment of emission. If the transition moments are collinear, the anisotropy is the highest. Since absorption transition moments to different electronic states may have different directions, the measured anisotropy will depend on the excitation wavelength. Consequently, anisotropy measured as a function of excitation wavelength will show information about the relative orientation of transition moments.

Emission anisotropy can be defined as in equation 13

$$r = \frac{I_{||} - I_{\perp}}{I_{||} + 2I_{\perp}},$$ (13)

where $I_{||}$ and $I_{\perp}$ are the intensity polarized emissions that have a polarization of the observed intensities parallel and perpendicular to the excitation light polarization. The limits of anisotropy

are between -0.2 to +0.4 [1-3]. The value of +0.4 or r_o is the theoretical anisotropy in the absence of any angular displacement in the relative direction of absorption and emission transition moments (absorption and emission transition moments are colinear). The value of anisotropy r is -0.2 is when both the absorption and emission transition moments are orthogonal, equation 14. There can be multiple processes contributing to transition moment reorientation besides the intrinsic difference between the directions of absorption and emission transition moments. This includes the Brownian molecule rotation or the resonance energy transfer. When the absorption and emission transmission moments are no longer colinear and form an angle α between them the anisotropy of the system is [27]

$$r = 0.4 \left(\frac{3cos^2\alpha - 1}{2} \right). \tag{14}$$

1.9 Lifetime

The excited state deactivation process can be described by rates of various deactivation Γ is the radiative rate and k_{nr} is the nonradiative rate. These are probability rates (probability of the given process per unit of time), and the emission process is a statistical phenomenon. So, the emission lifetime depends on a sum of all deactivation rates of an excited state. As shown in Figure 2, the cumulative deactivation rate of a singlet excited state is $\Gamma + k_{nr} + k_{ISC}$ where we separated the nonradiative rate of intersystem crossing, k_{ISC}. We can now define the characteristic lifetime of a singlet state as

$$\tau = \frac{1}{\Gamma + k_{nr} + k_{ISC}}. \tag{15}$$

The deactivation process (for fluorescence or phosphorescence) is a statistical process, and the lifetime represents the average time the excited molecule spends in the excited state. When

working with a large number of molecules, the number of molecules in the excited state as a function of time, N(t), can be described as [1, 2]

$$N(t) = N_0 e^{-\frac{t}{\tau}}, \tag{16}$$

where N_0 is the initial population of the molecules in the excited state, t is time, and τ is the lifetime defined as time after which the population of excited molecules decreases e times ($N(\tau) = N_0 e^{-1} = 0.368 N_0$ or 36.8% of N_0 remain in the excited state). Henceforth the fluorescence intensity is directly proportional to the number of molecules in the excited state, and the time-dependent emission intensity, I, can be described as

$$I(t) = I_0 e^{-\frac{t}{\tau}}. \tag{17}$$

A graphical representation of a single exponential intensity decay as a function of time is presented in Figure 8. The intensity on a logarithmic scale (left side) corresponds to a slope of $1/\tau$.
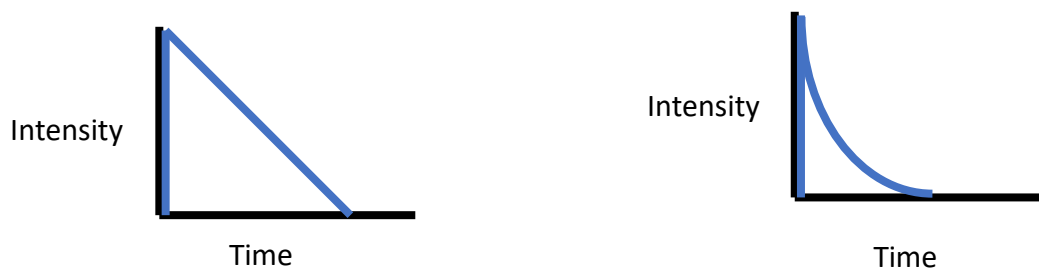
Figure 8. An example of a monoexponential lifetime decay curve on log scale (left) and linear scale (right).

1.10 Phosphorescence

As previously mentioned, transitions from excited triplet to the singlet ground state are forbidden. As a result, the deactivation rates from a triplet state are several orders of magnitude smaller than those for fluorescence. Consequently, the phosphorescence lifetimes ($\tau = 1/\Gamma_p + k_{nr}$) are much longer than fluorescence lifetimes.

When one of the two electrons of opposite spins (belonging to a molecular orbital of a molecule in the ground state) is promoted to an antibonding molecular orbital (excited state of higher energy), its spin remains unchanged. The total spin quantum number, S ($S = \sum s_i$ with s_i= +1/2 or -1/2) remains equal to zero. Because the multiplicities of both ground and excited states (M = 2S+1) are equal to 1, both states are called the singlet state. The energy of a triplet state is lower due to having the two electons being farther apart. This causes less coulombic repulsion than the singlet excited state, and phosphorescence emission $T_1 \rightarrow S_0$ is generally shifted to longer wavelengths relative to fluorescence; hence the Stokes shift is much larger.

17

The transition from a singlet state to a triplet state is forbidden and should never happen in a purely electronic system. However, molecules are built from multiple, different atoms, and there is a potential for a weak interaction between the orthogonal states of different multiplicities. The presence of heavy atom(s) (such as iodine and bromide) in a molecule can perturb the electronic structure of a molecule facilitating intersystem crossing and thus enhancing the probability of phosphorescence emission. If the singlet excited state converts into a state where the promoted electron has changed its spin parallel to each other, their total multiplicity M will change. The change in multiplicity results from the total spin quantum number equaling 1 and the multiplicity 3, thus the triplet state. The efficiency of the coupling varies with the fourth power of the atomic number, hence why the presence of a heavy atom favors intersystem crossing from singlet to triplet.

1.11 Indoles and Tryptophan

Indole is an aromatic heterocyclic organic compound with the chemical formula C_8H_7N, and the structure is shown in Figure 9. It has a bicyclic structure, consisting of a six-membered benzene ring fused to a five-membered pyrrole ring. Indole is an aromatic part of an essential amino acid, tryptophan (TRP), that is responsible for the UV-Vis spectral properties of this amino acid. Tryptophan (TRP) is an essential amino acid with sound absorption and intense fluorescence, presenting favorable spectroscopic properties. Furthermore, tryptophan is not common and is present in small numbers in most functional proteins. Even fairly large proteins like myoglobin contain two TRPs, human serum albumin (HSA) contains a single TRP, or tetrameric hemoglobin contains 6 TRPs (single in each β-subunit and two in each α-subunit). So, for a long time, there has been a lot of effort to use the spectroscopic properties of tryptophan (absorption and emission) to study proteins and protein interactions. Also, for many years special attention has been paid to

TRP room temperature phosphorescence (RTP) [16, 20, 59]. The advantage of using intrinsic TRP emission (fluorescence and phosphorescence) is that there is no need for any protein modification or substitution. TRP fluorescence has been broadly employed for many years in studying protein systems, including protein dynamics and conformational changes [20, 23, 41, 57]. It has proven immensely useful for studying a broad range of macromolecular processes. The fluorescence lifetime of TRP depends on its environment and ranges from picosecond to nanoseconds time scale. This limits the range of dynamic studies (e.g., time-resolved anisotropy decay of TRP moiety [16-18]) to tens of nanoseconds.

A chemical scheme of tryptophan is shown below in Figure 9.
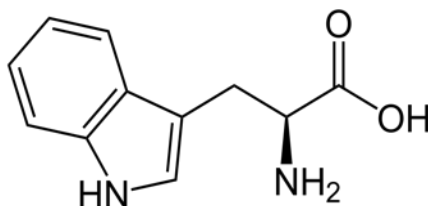
Figure 9. Chemical structure of the amino acid tryptophan.

Indole's photoluminescence was researched to understand the mechanisms of tryptophan's phosphorescence lifetime [21, 22]. Various substituted atoms in the indole ring significantly affect its photoluminescent properties. Heavy atom substitutions, in particular, promote electronic structure perturbations that lead to highly attenuated fluorescence and enhanced intersystem crossing leading to enhanced phosphorescence emission. Importantly, indole and its derivatives present good, convenient phosphorescence in a solid matrix and might allow for the study of different conditions (environmental and external like EM field) affecting molecular systems that might lead to enhanced ISC and highly enhanced phosphorescence.

In Figure 10, various studied indole derivatives are presented.
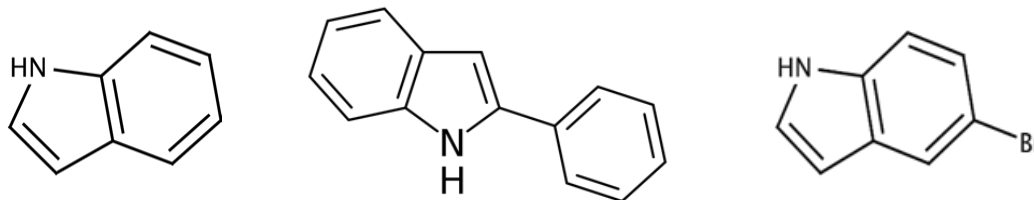
Figure 10. Chemical structure of indole (left), 2-Phenylindole (middle), and 5-Bromoindole (right).

2-Phenylindole (2PI) is indole with benzene covalently bound to the second carbon shown in the middle of Figure 10. 5-Bromoindole is another indole, but a bromide ion is covalently bound to the fifth carbon on the right of Figure 10. These two indole derivatives were chosen in this study because they increase the intersystem crossing rate to increase the phosphorescence radiative rate.

1.12 Polyvinyl Alcohol

Polyvinyl Alcohol (PVA) is a transparent polymer that will be used to immobilize the indole, 2PI, 5-BrI, and TRP. The advantage of using PVA for embedding the molecules is the low permeability to oxygen that limits oxygen quenching and increases fluorophore structural stability, allowing for long-lived phosphorescence to be visible/measurable.

Chapter 2 Methodology

2.1 Materials

Indole, 2-Phenylindole (2PI), 5-Bromoindole (5-BrI), tryptophan (TRP), poly (vinyl alcohol) (PVA) [molecular weight of 130,000 atomic mass unit (amu)], and HPLC grade methanol were all sourced from Sigma Aldrich, Inc (USA). Upon arrival, the indoles and tryptophan have a purity of 98%. However, to minimize impurities in the samples, the indole, 2PI, 5-BrI, and TRP were recrystallized multiple times with a 50:50 mix of methanol and deionized (DI) water until the samples became snow-white in color. The recrystallization procedure [89] is based on the principle that the solubility of most solids increases with increased temperature. As temperature increases, the amount of solute that can be dissolved in a solvent increases. An impure compound is dissolved (the impurities could also be soluble in the solvent) to prepare a highly concentrated solution at a high temperature. The solution is cooled. Decreasing the temperature decreases the solubility of the compound, and the excess solute crystalizes (is excluded from the solution, forming crystals).

In most cases, compound crystallization allows only the same type of molecules to be built into the crystal structure. The impure substance will crystallize having a much higher purity because the impurities won't be accepted/incorporated into an ordered crystal structure of the compound, leaving the impurities behind in the solution. The process is typically repeated multiple times. An example of recrystallization of 5-BrI is shown below in Figure 11.
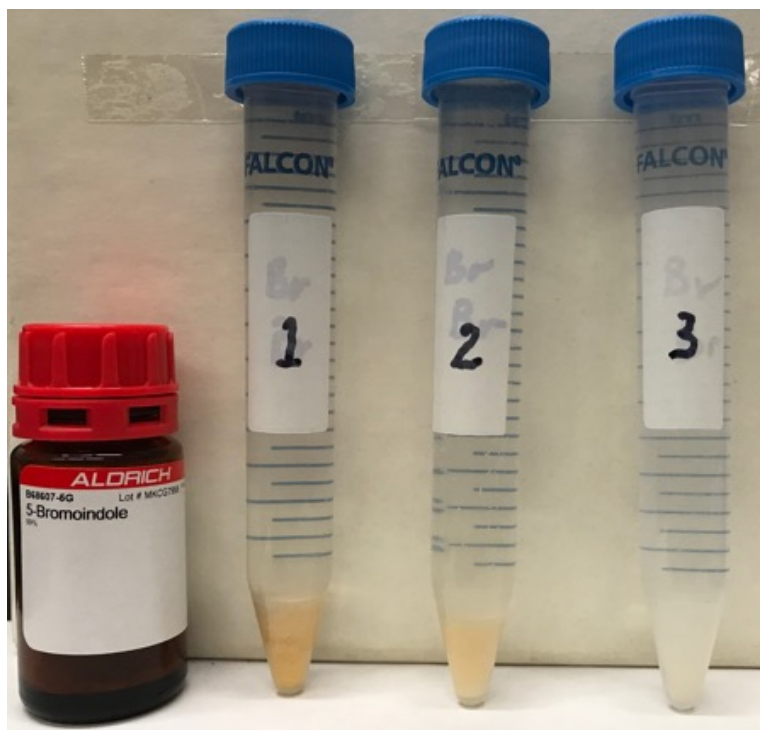
Figure 11. 5-Bromoindole's (98% purity) recrystallization process. Vial 1 is 5-Bromoindole as is from the vial in a 50:50 mix of methanol and DI water. Vial 2 is obtained after several recrystallization runs. The impurities are visibly fading. Vial 3 is the finished product of recrystallization.

Stock solutions of indole, 2-Phenylindole, 5-Bromoindole and tryptophan were prepared from compounds purified via the recrystallization process in ethanol.

2.2 Poly (vinyl alcohol film) preparation

Poly (vinyl alcohol) from Sigma Aldrich, Inc. (USA) with a molecular weight of 130,000 atomic mass units was used for the experiments. PVA films were prepared according to the procedure described in the literature [8-11]. Briefly, double distilled water (600 mL) was added to a 1000 mL flask containing a magnetic stirring bar. PVA powder (60 g) was slowly added under stirring and heated to 90°C, and the stirring continued for 4 hours. The PVA powder dissolves, and

the resulting homogeneous, well-transparent solution was allowed to cool to room temperature overnight to remove all the bubbles. A few mL of a stock solution of one of the dyes (Indole, 5-BrI, 2PI, TRP) in water or ethanol was added to a freshly prepared PVA solution (~6.0 mL in a 20 mL glass vial) at 50ºC. The mixture was thoroughly mixed for 5 minutes to assure complete mixing, followed by sonication for 3 minutes to remove all the bubbles that formed during the mixing. Next, the mixture was poured into a 2-inch diameter plastic petri dish on a flat and balanced surface and kept in a moisture-free, dark environment for 4 to 6 days to allow film drying. The dry films were removed from the dish and stored in dry conditions.

2.3 Spectroscopic Measurements

2.3.1 Absorption Measurements

UV-Vis absorption was measured in a Cary 60 UV-Vis spectrophotometer (Agilent Technologies, Inc. (USA)). Sample films were measured multiple times (average of 5 runs), and absorbances were averaged. The baseline for absorption measurements was taken from the PVA-only film.

2.3.2 Fluorescence Measurements

Steady-state fluorescence spectra were measured in a Varian Cary Eclipse spectrofluorometer (Agilent Technologies, Inc. (USA)). This device is equipped with a grid ultraviolet (UV) polarizer on excitation and a plastic (sheet) polarizer on the emission path.

2.3.3 Phosphorescence Measurements

Phosphorescence measurements were carried out on a Varian Cary Eclipse spectrofluorometer using phosphorescence mode. Shown below in Figure 12 is the concept of phosphorescence measurements.
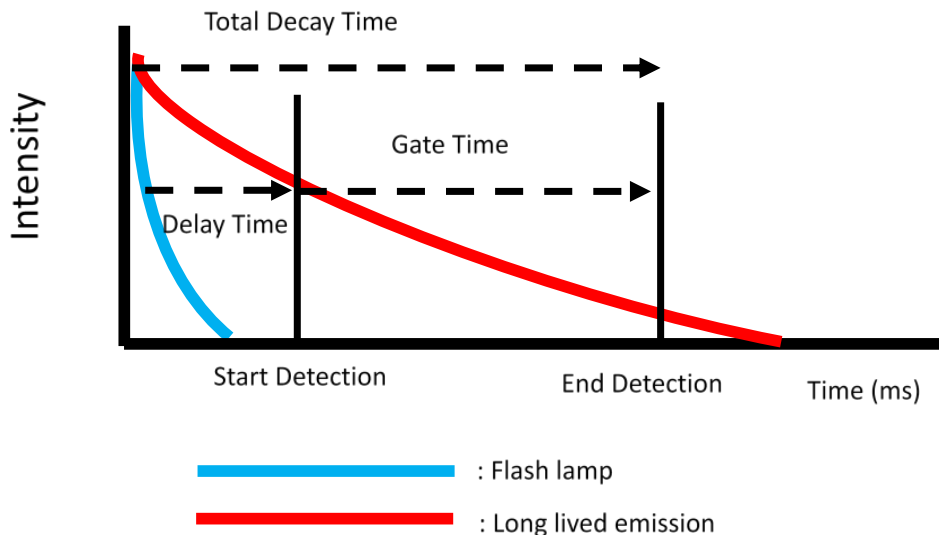
Figure 12. Parameters used for phosphorescence measurements on the Varian Cary Eclipse. Delay time is the time that elapses between the last flash of lamp excitation and the beginning of the data collection. Gate time is the overall reading time of the emission signal after the delay time. The number of flashes is how many times the sample gets excited by the flash lamp per cycle. The total decay time is the time for the phosphorescence signal to decay to approximately zero, typically delay time + gate time.

Phosphorescence measurements use a time gating approach to suppress the short-lived fluorescence emission and excitation light scattering. All parameters (delay time, gate time, number of flashes, and total decay time) are graphically represented in Figure 12 and described in the caption of Figure 12. The parameters used are mentioned in the results section for each sample.

2.3.4 Lifetime Measurements

Lifetimes were measured on the FluoTime 300 (FT300) fluorometer (PicoQuant, GmbH). The FT300 is equipped with an ultrafast microchannel plate (MCP) photomultiplier tube (PMT) (Hamamatsu, Inc. (Japan)) detector. Time-Correlated Single Photon Counting (TCSPC) was performed with a PicoHarp 300 (Picoquant, GmbH (Germany)) for fluorescence intensity decays. A TimeHarp 260 card was used for TCSPC phosphorescence intensity decays. The intensity decays were analyzed using the FluoFit (version 4.6) program from PicoQuant (GmbH (Germany)) using a multi-exponential fitting model for the intensity decay I(t),

$$I(t) = \sum_i \alpha_i e^{-\frac{t}{\tau_i}}, \tag{18}$$

where α_i is the fractional amplitude of the intensity decay of the ith component at time t and τ_i is the lifetime of the ith component. Calculations of the intensity ($< \tau >_{int}$) and amplitude ($< \tau >_{amp}$) average lifetimes were as follows:

$$< \tau >_{int} = \sum f_i \tau_i, \tag{19}$$

$$< \tau >_{amp} = \sum \alpha_i \tau_i, \tag{20}$$

$$f_i = \frac{\sum \alpha_i \tau_i}{\sum \alpha_i}, \tag{21}$$

where f_i represents the fractional intensity for each lifetime component.

The reduced χ^2 for least-squares fitting analysis [1, 84-86] is performed according to Equation 22,

$$X_R^2 = \frac{1}{n-p} \sum_{j=1}^{n} \left[\frac{I_{ob}(t_j) - I_{cal}(t_j)}{\sigma_j} \right]^2, \tag{22}$$

where n is the number of observations (this is the number of detected photons in a decay curve), p is the number of floating parameters, $I_{ob}(t_j)$ is the intensity measured at time t_j, $I_{cal}(t_j)$ is the theoretical value for the fitted intensity decay at time t_j, and σ_j is the standard deviation.

For the time-resolved analysis, one of the most common approaches to evaluate the range of estimated parameters is the support plane analysis procedure. When running a regular analysis with all floating parameters yields' a minimum (smallest) value of X_R^2 or $X_R^2(min)$. To examine the quality of estimated parameters, one can monitor changes in the value of X_R^2 when one parameter is varied around its initial estimated value. In practice, the idea is to fix one parameter to a value different from its best estimate and then rerun the least-square analysis allowing the other parameters to adjust to a new minimum with the new value of X_R^2. This new value is obtained with one fixed parameter we call $X_R^2(fp)$. We increase the value of the fixed parameter and repeat this routine each time, allowing all other parameters to adjust to a new minimum. The procedure is repeated until the $X_R^2(fp)$ value for a given value of the parameter exceeds an acceptable value. Typically, the routine is repeated until the new value $X_R^2(fp)$ exceeds the value predicted by F-statistics for a given number of parameters (p), the number of degrees of freedom (NFD), and the chosen probability level, P. Probability, P, describes the probability that the value of the F-statistic (ratio of chi-squares for two fits) is due to only random error in the data related to the standard deviation of the experiment. For a one-standard-deviation confidence interval, the value of P is approximately 67%; for two-standard deviation confidence intervals, the value of P increases to about 95%. F is expressed as

$$F = \frac{X_R^2(fp)}{X_R^2(min)} = 1 + \frac{p}{NFD} F(\alpha_i, \tau_i, NFD, P), \qquad (23)$$

where $F(p, NFD, P)$ is the F-statistic value with parameters α_i, τ_i and NFD with a probability of P. Values of F-statistics can be found in the literature.

For example, the support plane analysis below shows the lifetime of the dye F7GA in ethanol.
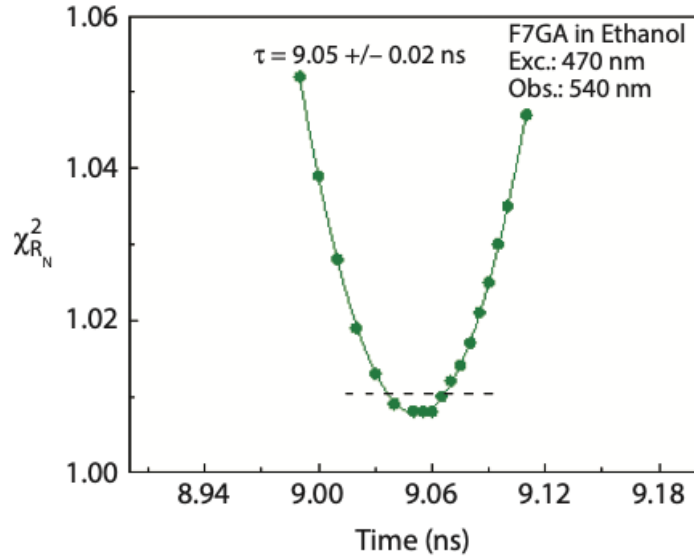
Figure 13. The support plane analysis (X_R^2 analysis) of Fluorol 7GA in ethanol lifetime. The dashed horizontal line corresponds to 67% of confidence. In TCSPC, this confidence corresponds to about 1.01 value of normalized X_R^2.

The recovered lifetime from the analysis program FluoFit (Picoquant, GmbH, Germany) reveals a lifetime of 9.05 ns with an accuracy of $\pm 0.02\ ns$. The error was estimated by fixing the lifetime at values near the lifetime of 9.05 ns and repeating the analysis. At each fixed value, we recorded X_R^2. After normalization (ratio of $X_R^2/X_R^2(\min)$) we plot the dependence of normalized $X_{R_N}^2$ as a function of a lifetime, as shown in Figure 13. In this case, and for most single-exponential decays, the dependence of normalized X_R^2 on the fixed lifetime is a symmetric

27

parabola. Therefore, the lower-and upper-confidence intervals are identical, and we can estimate the accuracy of the error ($\pm$). In more complex decays, the parabolic dependence is often not symmetrical and the lower confidence can be different from the upper confidence interval.

2.3.5 G-factor

Commercial instruments have a bias toward light polarization. This bias means that the detection path (monochromator, photomultiplier tube (PMT) detector, and collection optics) responds differently depending on the light polarization (vertical or horizontal), thus requiring a correction. Calibrating the system for the skewed response of the detection system is done by comparing the vertical and horizontal light relative to each other. This calibration is known as the G-factor correction. The G-factor is a wavelength-dependent factor that calculates the machines' inability to correctly detect light polarization (horizontal or vertical) and adjust the relative value of one component to the value of another orthogonal component. We need to know relative intensities for vertical and horizontal intensity components to calculate the G-factor.

The question arises of how to correct the uneven transmission (polarization) through the detection system of the spectrofluorometer. We need to know the relative intensities for vertical and horizontal components to find a correction factor. One possible way to know the relative intensities for vertical and horizontal components is to simply have isotropic emission. In such a case, both components should be equal. For square geometry, this can be realized with horizontal excitation. In Figure 14, we show the coordinates for a square geometry with vertical (A) and horizontal (B) excitations in which we inserted the distributions of excited molecules. For the vertical excitation, the distribution of excited molecules seen from the observation direction, Figure 14 (left), is dumbell shaped as described by the $\cos^2\omega$ photoselection rule. For the

horizontal excitation, the distribution of excited molecules seen from the observation direction (along the x-axis) is symmetrical with equal vertical and horizontal components.
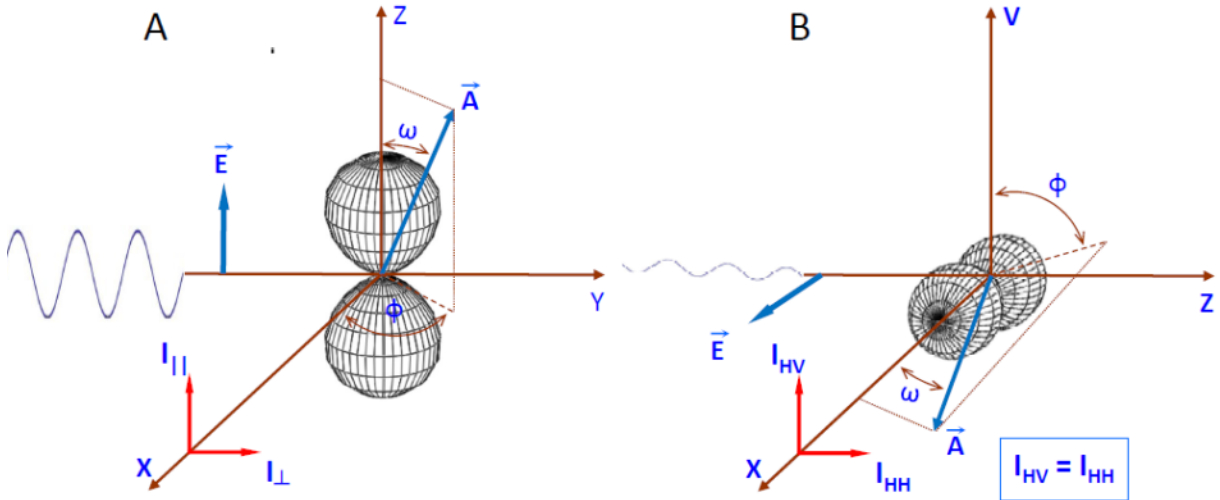
Figure 14. (Left) the distribution of the fluorophore's excited dipoles with a vertically polarized excitation. The shape is a result of photoselection. (Right) the distribution of the fluorophore's excited dipoles with a horizontally polarized excitation. The observed fluorescence looks isotropic with equal vertical and horizontal polarization components.

So the I_{HV} and I_{HH} are equal, and we can use horizontally polarized excitation light for which two (vertical I_{HV} and horizontal I_{HH} components should be equal) to find the G-factor. The wavelength-dependent G-factor can be calculated from the relation,

$$G(\lambda) = \frac{I_{HV}(\lambda)}{I_{HH}(\lambda)},$$

(24)

where $I_{HV}(\lambda)$ is the polarized fluorescence intensity component measured with the excitation polarizer turned horizontal at any given wavelength and the emission polarizer turned vertical. $I_{HH}(\lambda)$ corresponds to the intensity at any given wavelength in a case where both excitation and the emission polarizers are horizontal.

This method of the G-factor correction can only be used for a square geometry. In the case of a non-square geometry configuration, or front face (FF), shown in Figure 15, a different method is used.
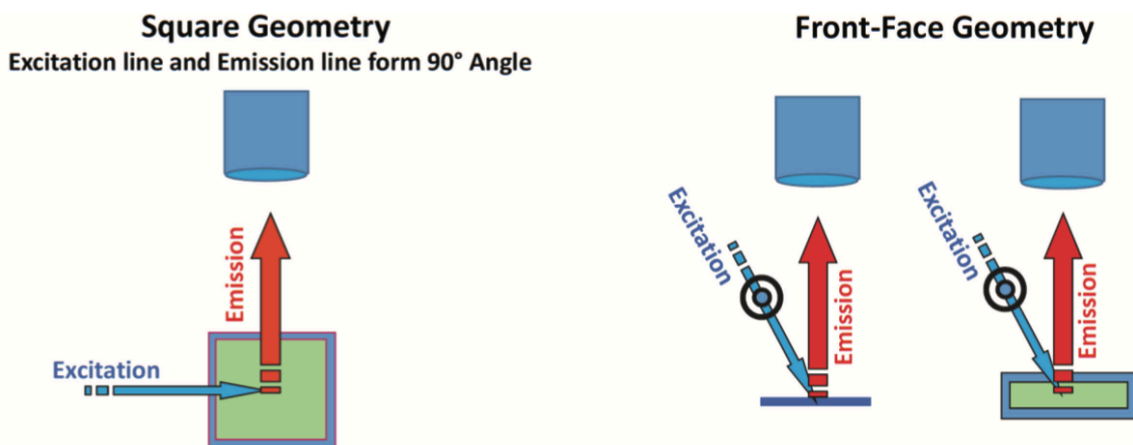
Figure 15. (Left) typical commercial spectrofluorometer set up for fluorescence measurements. (Right) front face geometry used for measuring fluorescence/phosphorescence emission of films.

For FF configurations rotating, the excitation polarization will not yield equal intensities for vertical and horizontal components. In this case, we can use fluorophores, for which we expect the distribution of excited dipoles is completely randomized before emission. This can happen when fluorescence lifetimes are long and fluorophores are in low viscosity solvents. The correlation time is much shorter than the fluorescence lifetime, and fast rotating molecules will quickly randomize. As an example, we can use the emission of anthranilic acid (AA), dansyl amide (DA), and ruthenium (Ru) in ethyl acetate (low viscosity). Figure 16 shows the fluorescence intensities measured for these dyes with vertical and horizontal observations when the system was excited at 360 nm. The emission should be isotropic, and the expected intensity components (vertical and horizontal) should be equal.
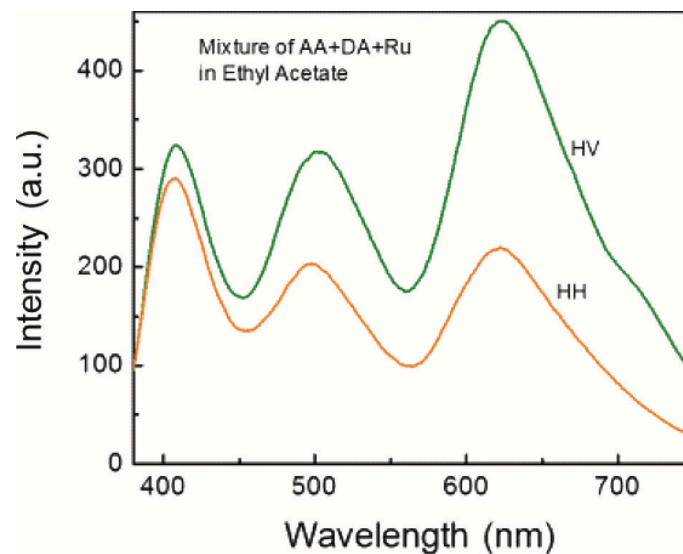
Figure 16. Emission of mixed AA, DA, and Ru in front face configuration with an excitation of 360 nm.

Now the calculated G-factor per wavelength is as follows in Figure 17.
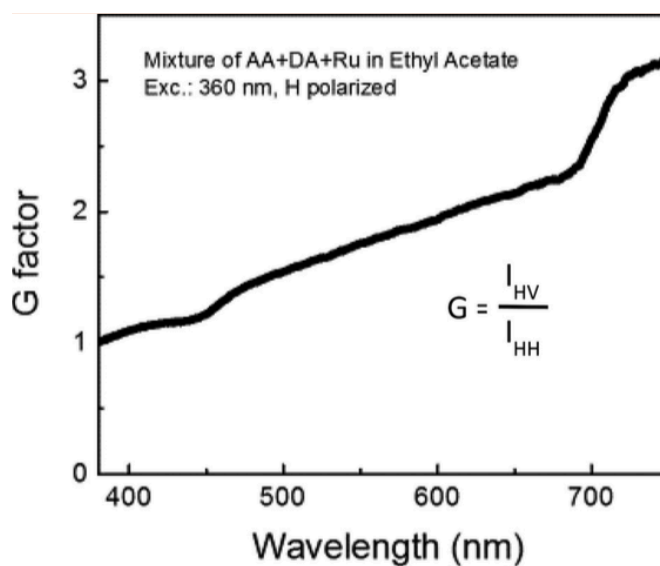
Figure 17. The G-factor was calculated using a horizontally (H) oriented polarizer in the excitation path.

For the square geometry G-factor calculation the following fluorophores were used, 2-aminopurine (2AP) (320 – 400 nm), 2,5-bis-(4-biphenylyl)-oxazol (BBO) (400 – 475 nm), coumarin 153 (C153) (475 nm – 575 nm), and ruthenium (Ru) (575 – 700 nm).
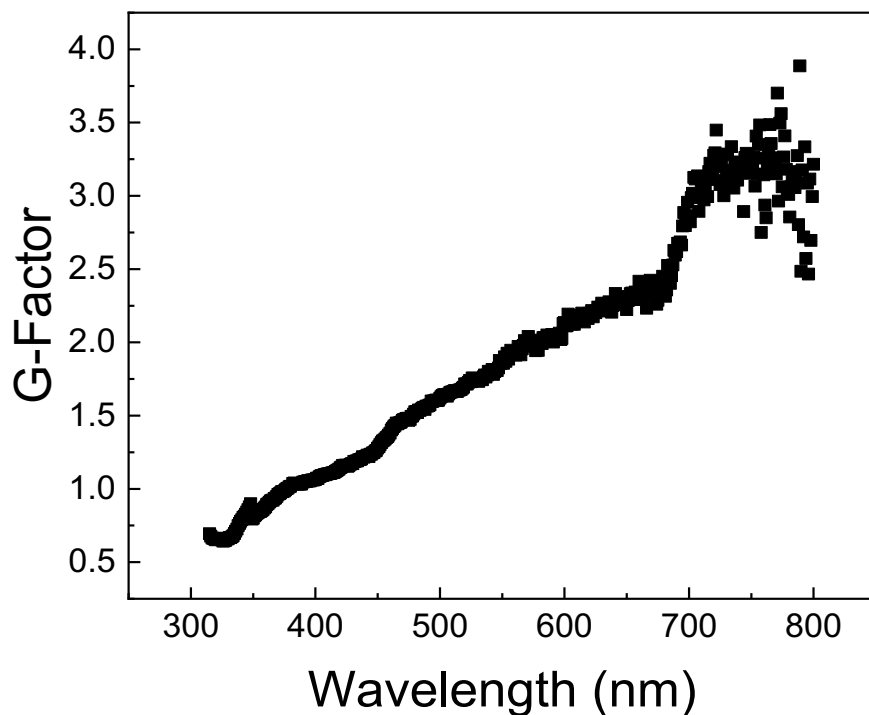
Figure 18. G-factor of the Varian Cary Eclipse spectrofluorometer in square geometry.

Both Figures 17 and 18 show similar G-factor curves for either case. The wavelengths starting from 400 nm and up show the instrument bias increasing as the wavelengths gets closer to the red. The corrected anisotropy calculation as a function of the wavelength is

$$r(\lambda) = \frac{I_{VV}(\lambda) - G(\lambda) * I_{VH}(\lambda)}{I_{VV}(\lambda) + 2 * G(\lambda) * I_{VH}(\lambda)}, \tag{25}$$

where I_{VV} is the intensity measured with a vertical polarization on excitation and a vertical polarization on emission, I_{VH} is the intensity measured with a vertical polarization on excitation and a horizontal polarization on emission, and G is the G-factor value at a given wavelength.

2.3.6 Quantum Yield

The efficiency of the radiative process, quantum yield (QY) Q_Y, reflects the number of emitted photons compared to the total number of absorbed photons. This describes the probability that a molecule will emit a photon after absorption and corresponds to the ratio between the radiative rate and the sum of all rates

$$Q_Y = \frac{\Gamma}{\Gamma + k_{nr}}. \tag{26}$$

Importantly, in fluorescence, we do not use energy efficiency since the wavelength of emission is typically longer than the wavelength of excitation light (Stokes shift), which already reflects energy being lost. A $Q_Y = 1$ typically does not mean energy efficiency is equal to 1; it only means that each absorbed photon leads to the emission of a photon typically of lower energy.

An important example where we should be careful how to analyze the results is when calculating the quantum yield (QY) of an unknown fluorophore. A simple way to evaluate the quantum yield for an unknown dye is to compare it with a reference (compound for which QY is known). Equation 26 (above) defines the quantum yield as a ratio of emitted photons to absorbed photons by the sample or equivalently defines quantum yield through the radiative and non-radiative rates. There is no simple way to evaluate/calculate the quantum yield of an unknown fluorophore. The reason for that is that we will need to have a perfectly calibrated excitation lamp to know precisely the number of photons emitted by the lamp per second and a perfectly calibrated detection system that will be able to exactly evaluate the total number of emitted photons (photons

emitted in all directions). For evaluating the total number of emitting photons, integrated spheres are sometimes used, but this does not always give satisfactory results. In general, the emission of the fluorophore (number of emitted photons) is proportional to the number of absorbed photons and the fluorophore quantum yield. Photons are emitted in all directions (and only a small part reaches the detector), and photons are spread through the emission spectrum. Using a known standard/reference in the same configuration as our unknown sample, we can safely assume that the portion of photons emitted toward the detector from our sample is the same. So, in principle, it is sufficient to measure absorptions for the reference and sample and then emission spectra in identical conditions (if the spectral range is different, we need to recalculate the number of detected photons properly). The number of absorbed photons equals the number of excited molecules per unit of time and is proportional to the change in the intensity of light going through the sample. According to the Beer-Lambert law (equation 6), the number of absorbed photons (excited molecules) of the standard will be

$$N_R \sim \Delta I_R = I_0(1 - 10^{-OD_R}), \tag{27}$$

and for the sample

$$N_S \sim \Delta I_S = I_0(1 - 10^{-OD_S}), \tag{28}$$

where OD_R and OD_S are optical densities (absorbances) for the reference and sample, respectively. The number of emitted photons for the reference and sample will be

$$N_R^{Ph} = N_R QY_R \tag{29}$$

and

$$N_S^{Ph} = N_S QY_S. \tag{30}$$

A typical system does not collect all the photons. However, for a system with the same detection configuration (same system and the same/identical cuvette), the fractions of collected photons for the reference and sample should be identical if the samples have the same refractive indexes. As it is relatively easy to keep the detection geometry constant, our sample and reference are frequently in different solvents with different refractive indexes. To discuss how this may affect our signal and how to correct for this effect, let us consider the configuration presented in Figure 19.
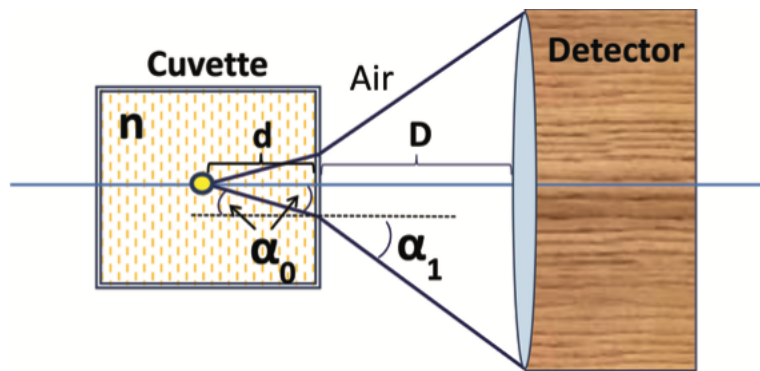
Figure 19. Reflection of light exiting a cuvette. At a higher refractive index, the light exits the cuvette at a larger angle and the lens collects less light.

The reference is in the solution with a refractive index, n_R, and the sample refractive index n_S. The emitting point in the center of the cuvette is located at a distance d from the cuvette wall and emits uniformly in all directions. The detector is at a distance D (D>>d) from the cuvette. For a fixed geometry, the system will always see the light entering into the detector (collecting lens) under the angle α_1. Due to refraction, this will correspond to the angle α_0 that will depend on the refractive index, n, of the solvent in the cuvette. Only the light emitted from a point source into the cubical angle α_0 will reach the detector. At any given distance, the intensity I is distributed

on a surface $4\pi d^2$ and the portion of energy flowing to the detector is proportional to the surface

area covered by the angle α_0, $s = \pi r^2 = \pi(d\sin(\alpha_0))^2$ and using the notation as in Figure 19

(cuvette) for sample and reference, we will get

$$S_0^R = \pi D^2 tg^2 \alpha_0^R \tag{31}$$

and

$$S_0^S = \pi D^2 tg^2 \alpha_0^S \tag{32}$$

Where we assumed $D \approx D + d$. Snell's law lets us calculate angles for a reference $\sin\alpha_0^R =$

$n_R\sin\alpha_1$ and for a sample $\sin\alpha_0^S = n_S\sin\alpha_1$. We can now write the number of photons emitted

toward the detector at a given wavenumber (wavelength) by reference and sample, respectively,

$$N_R^{Ph}(v) = \frac{N_R QY_R}{4\pi R^2}\pi D^2 n_R^2 tg^2 \alpha_1 \tag{33}$$

and

$$N_S^{Ph}(v) = N_S QY_S \pi D^2 n_S^2 tg^2 \alpha_1. \tag{34}$$

We can use the wavelength or wavenumber scale to calculate the total number of photons

emitted by the sample. The total number of emitted photons is proportional to the area under the

emission spectrum. We can then enter it in equations 33 and 34, and by comparing signals

measured for reference and sample, we can calculate the quantum yield of the sample

$$QY_S = QY_R \frac{(1-10^{-OD_R})n_S^2 \int F_S(v)dv}{(1-10^{-OD_S})n_R^2 \int F_R(v)dv}, \tag{35}$$

where $F_S(v)$ and $F_R(v)$ are integrated intensities (areas under the emission spectra profile) for

sample and reference, respectively. The spectrum profile will generally include a detector

sensitivity factor (correction for a different sensitivity to a different wavelength). Equation 35

lets us calculate the quantum yield of a sample if we know the quantum yield of the reference. We do not have to worry about differences in the sample and reference absorptions in this general representation.

For most monochromators (with gratings as dispersing elements), the linear step will be in wavelength, and we will use the wavelength version of equation 35

$$QY_S = QY_R \frac{(1-10^{-OD_R})n_S^2 \int F_S(\lambda)d\lambda}{(1-10^{-OD_S})n_R^2 \int F_R(\lambda)d\lambda}.$$ (36)

Chapter 3 Results and Discussion

Most of the presented results have already been published by us [8-11], and we only present crucial findings with general conclusions. As a reminder, the following indole derivatives were chosen, indole, 2-Phenylindole, and 5-Bromoindole. The idea of possibly directly exciting the triplet state $(S_0{\rightarrow}T_1)$ was still perceived as an impossible task. Specifically, why these indole derivatives were chosen because they all have known photoluminescent (fluorescence and phosphorescence) properties. Indole, for starters, is a simple molecule and the photoluminescent backbone for the amino acid tryptophan. Indole's photoluminescent properties will be studied first on the results page.

3.1 Indole Results

The results below will follow a pattern of studying each molecule's photoluminescent properties. First, the absorption spectra of the molecule will be observed to measure where light interacts $(S_0{\rightarrow}S_1)$ with the molecule. Next, the fluorescence emission and lifetime will also be observed. The fluorescence lifetime will show that the emission time domain will be in the nanosecond range. Phosphorescence emission through UV and direct excitation wavelengths will be observed and compared within their spectral region. Phosphorescence emission anisotropy will be studied to see if the difference in the angle between the absorption and emission transition moment will be low (high anisotropy). Both emission anisotropies will be compared to the UV excitation (low anisotropy) and direct excitation (high anisotropy). A high phosphorescence anisotropy will show that the absorption transition moment of phosphorescence is being excited. Phosphorescence excitation anisotropy will be measured to determine if the direct excitation wavelength is the most efficient wavelength of high anisotropy. Phosphorescence lifetimes will be measured between the UV and direct excitation wavelengths to show their time-domain being emitted will be in the

millisecond range. Lastly, temperature dependence is shown that phosphorescence is heavily sensitive to temperature, a common feature of phosphorescence.

3.1.1 Absorption and Fluorescence

The absorption spectrum of indole in PVA film at 20 °C is shown below in Figure 20. Inset within the Figure is the chemical structure of indole. The spectrum shows a structured absorption with the band maximum in the UV at 275 nm.
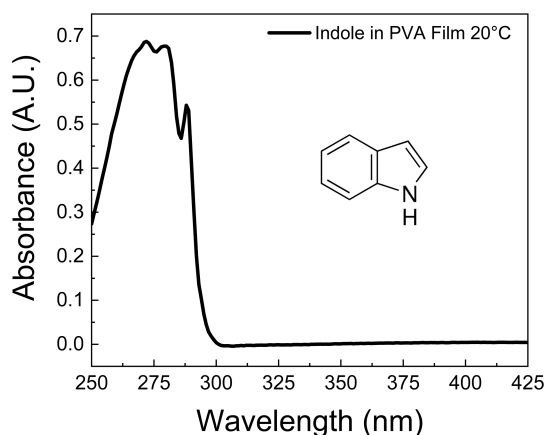
Figure 20. The absorption spectrum of indole in PVA film. The thickness of the film is about 0.3 mm.

The indole fluorescence in PVA film is also similar to indole, and its derivatives spectra in solutions and the emission peak position corresponds to a medium polar solvent [29]. Its emission spectrum is shown below in Figure 21 as the black line. Its fluorescence maximum is at about 325 nm. This is significantly shifted toward shorter wavelengths compared to the indole in water (about 360 nm). The fluorescence of PVA-only film (red line) is negligible, even with a UV excitation. If one focuses on the 450 to 500 nm range, as shown in the inset in Figure 21,

there is a slight evidence of another band. This is where phosphorescence would be expected [21,25,28,30].
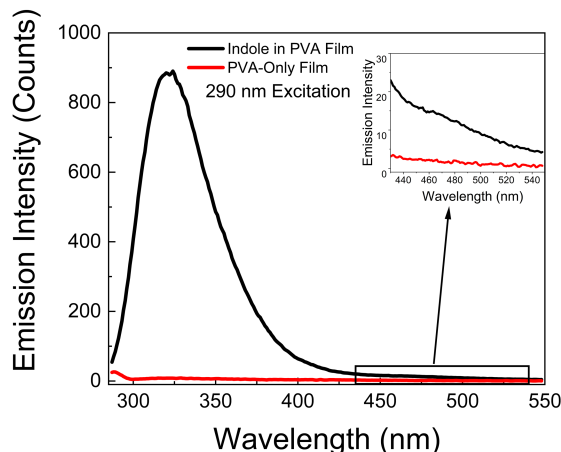
Figure 21. Fluorescence spectrum of indole in PVA film. The excitation was 290 nm. The insert is the part of the emission spectrum with a slight indication of phosphorescence.

Indole and many of its derivatives have fluorescent lifetimes in the range of 4-7 ns [31]. Using a 290 nm LED excitation at 10 MHz, Figure 22 shows that the intensity decay observed near the fluorescence peak at 325 nm can be fitted with a single exponential decay of 4.78 ns. The indole fluorescence lifetime measurement was done with the UV LED, which has a relatively broad full-width half-maximum of about 0.5 ns (see its response function IRF). Regardless, the 4.78 ns recovered/fitted fluorescence lifetime very well matches the observed intensity decay of indole.
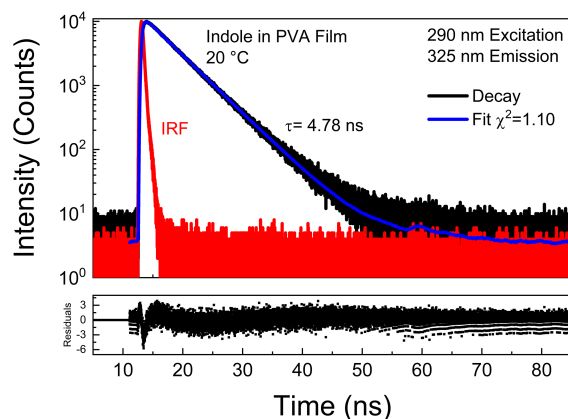
Figure 22. Fluorescence intensity decay of indole in PVA film. The decay can be fit to a single lifetime of 4.78 ns.

3.1.2 Phosphorescence

Emission spectra measured in phosphorescence emission mode for indole in PVA film excited at 290 nm (red line) are shown in Figure 23. Observed emission corresponds to the expected indole phosphorescence emission in the 400 to 600 nm range. 290 nm excites the singlet state of indole, a standard excitation route from the ground singlet state to singlet excited state, followed by intersystem crossing to the triplet state and then transitioning to the original ground singlet state that is associated with phosphorescence emission. Although there is no discernable absorption of indole in PVA film at 405 nm, as shown in Figure 20, it turns out that 405 nm light efficiently excites the indole triplet state leading to significant phosphorescence emission. In Figure 23, the phosphorescence emission excited with 405 nm light is presented as the black line. This emission is likely the result of the direct excitation of indole from the singlet ground state to the triplet excited state. A different polymer instead of PVA, PMMA (Poly (methyl methacrylate)), was used to show that direct excitation of indole does not occur just in the PVA matrix. Even if the extinction coefficient for the transition from the S_0 state to T_1 is very low (the absorption

41

spectrum cannot be measured), the population of the T_1 state with the xenon flash lamp is roughly comparable (about twice higher) to the population achieved through the intersystem crossing process. Such an efficient excitation of indole phosphorescence with blue light was an unexpected observation. A very weak trace of long-wavelength absorption can be identified in Figure 20, but it is very low and undiscernible within the thickness of the line.
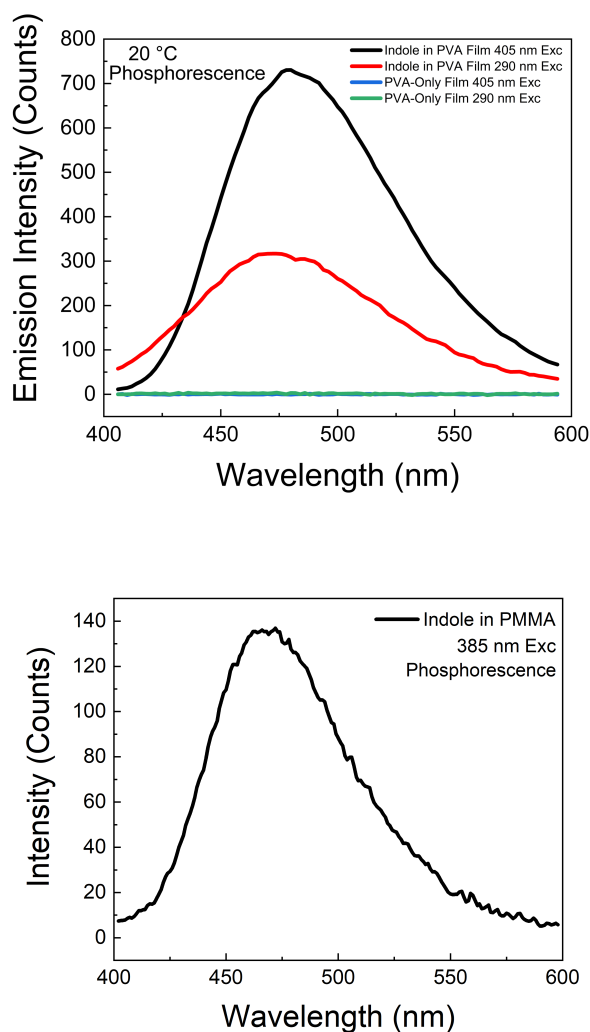
Figure 23. (Top) Room-temperature phosphorescence spectra of indole in PVA film with 290 nm (shown in red) and 405 nm excitation (shown in black). PVA-only film emission is shown as well

of 290 nm excitation (green) and 405 nm excitation (red). The bottom shows indole in PMMA with an excitation of 385 nm.

The $S_0 \rightarrow T_1$ absorption is well below any commercial spectrophotometer sensitivity. In order to determine where the indole in PVA film's phosphorescence could be excited, its phosphorescence excitation spectrum was measured and is presented in Figure 24. We want to stress that measurements in phosphorescence mode practically eliminate any excitation light scattering and background emission.
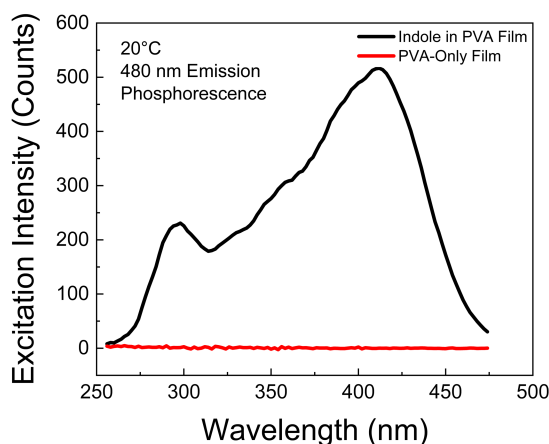
Figure 24. The room-temperature phosphorescence excitation spectrum of indole in PVA film (black line). The red line is PVA-only film. The observation was at 480 nm.

The phosphorescence excitation ranges from ~250 to 450 nm, with two distinct local maxima at 295 nm and 410 nm. The UV band in the excitation spectrum corresponds to the $S_0 \rightarrow S_1$ absorption and the band around 400 nm corresponds to the $S_0 \rightarrow T_1$ absorption.

3.1.3 Phosphorescence Lifetimes
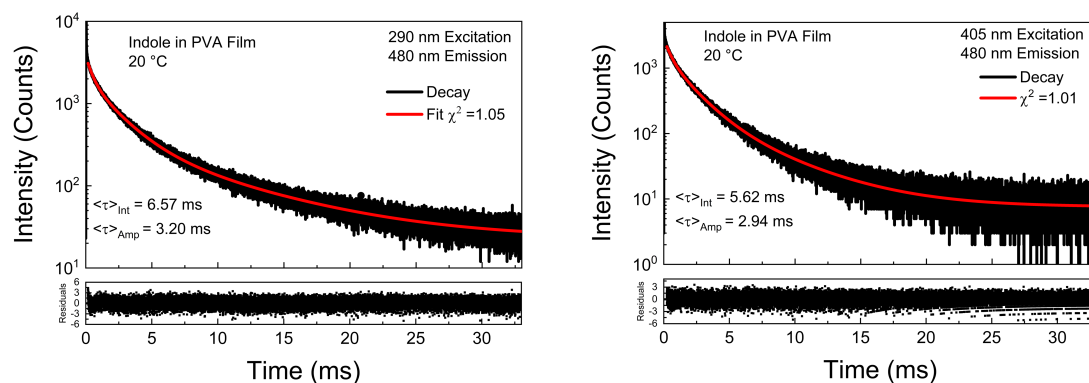
Figure 25. Room-temperature phosphorescence intensity decays of indole in PVA film with 290 nm excitation (left) and 405 nm excitation (right). The observation was 480 nm.

One additional characteristic parameter of phosphorescence emission is the lifetime of the triplet state (phosphorescence lifetime). To confirm that the observed indole emission with the 405 nm excitation is phosphorescence, we measured phosphorescence lifetimes of indole in PVA film with 290 nm excitation and 405 nm excitation. For this measurement, we used the FT300 system powered with a flash lamp with a repetition rate of 300 Hz. Measured intensity decays are shown in Figure 25. They both have complex intensity decays with similar millisecond lifetimes, as one would expect for phosphorescence. The lifetime analysis is shown below in Table 1. The lifetime with 290 nm excitation has an intensity averaged lifetime of 6.57 ms, while exciting with 405 nm has a lifetime of 5.62 ms. The small difference could be due to the time needed for the intersystem crossing process and relocation of the transition moment into an orthogonal orientation.

Parameter	Value (290 nm Excitation)	Value (405 nm Excitation)
$<\tau>_{Intensity}$ (milliseconds)	6.57	5.62
$<\tau>_{Amplitude}$ (milliseconds)	3.20	2.94
τ_1 (milliseconds)	10.53 ±0.21	9.17 ±0.09
α_1 (counts)	391.7 ±9.4	1080.5 ±16.1
τ_2 (milliseconds)	2.78 ±0.07	2.66 ±0.04
α_2 (counts)	1238.7 ±32.3	3484.0 ±55.4
τ_3 (milliseconds)	0.60 ±0.07	0.62 ±0.04
α_3 (counts)	907.2 ±91.6	2492 ±151

Table 1. Intensity and amplitude averaged lifetimes along with their three-component fits for both 290 nm excitation (Column 2) and 405 nm excitation (Column 3).

3.1.4 Phosphorescence Anisotropy

While the spectral difference between fluorescence and phosphorescence is apparent, along with the lifetimes being six orders of magnitudes different, a third aspect of the emitted light can also be measured that strongly suggests direct excitation to the triplet state for indole in PVA film, without the need for the usual intersystem crossing. With the typical UV excitation, the phosphorescence anisotropy is negative due to the orthogonal orientation of the phosphorescence transition moment with respect to the absorption transition moment (the $T_1 \rightarrow S_0$ transition moment is almost perpendicular to that of $S_0 \rightarrow S_1$). In Figure 26, we are presenting polarized phosphorescence emission components as measured with a vertical excitation light polarization (VV and VH). The horizontal component was corrected for the G-factor.
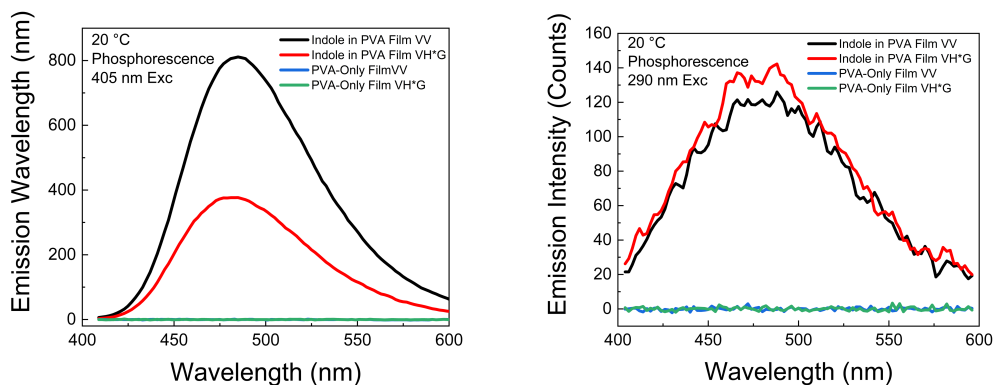
Figure 26. Polarized components of indole phosphorescence in PVA film. The excitations were 405 nm (left) and 290 nm (right). The PVA-only film spectra are shown as well.

On the left of Figure 26, indole in PVA film was excited using 405 nm, and the I_{VV} and I_{VH} components show a clear difference in their intensities. This means there is a non-zero positive, high anisotropy. When it was excited with 290 nm, as shown in Figure 26 (right), the VH component exceeded the VV component, which indicates a negative anisotropy. This is evidence of these two different excitations resulting in two different pathways to the triplet excited state T_1.
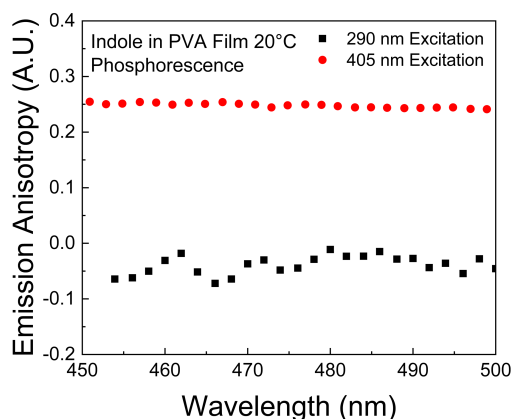
Figure 27. Phosphorescence emission anisotropy of indole in PVA film with 405 nm (shown as red dots) and 290 nm (shown as black dots) excitations.

Calculation of the emission anisotropy for both excitations 290 nm and 405 nm were done using equation 25. Figure 27 shows the anisotropy calculation as a function of wavelength of both excitations. With 290 nm excitation (black dots), the emission anisotropy is around -0.05. However, with 405 nm excitation, the emission anisotropy (red dots) is around 0.25.
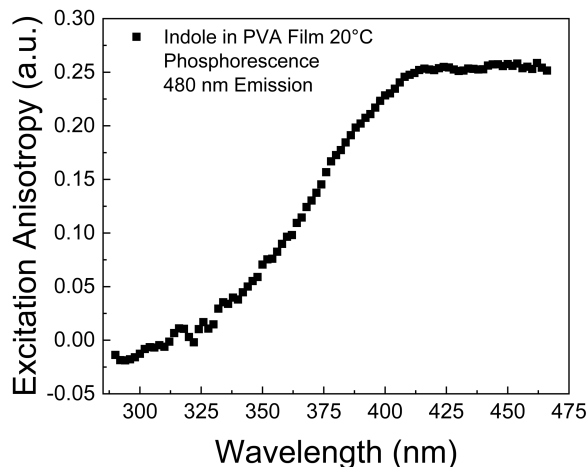
Figure 28. Phosphorescence excitation anisotropy. The observation was 480 nm.

The phosphorescence excitation anisotropy was measured to understand better where this change in anisotropy spectrally occurs, as shown in Figure 28. As expected, the anisotropy is low and negative when exciting in the 290-310 nm range. It transitions to the ~0.25 anisotropy around 400-450 nm excitation. This is evidence of a different excitation path.

3.1.5 Temperature Dependence

Finally, we compared the temperature dependences of indole in PVA film fluorescence and phosphorescence. In Figure 29 (A), the fluorescence spectra of indole in PVA film were measured at temperatures ranging from 10 °C to 60 °C. As shown in Figure 29 (C), the maximum intensities barely changed, as would be expected for fluorescence in a rigid medium.
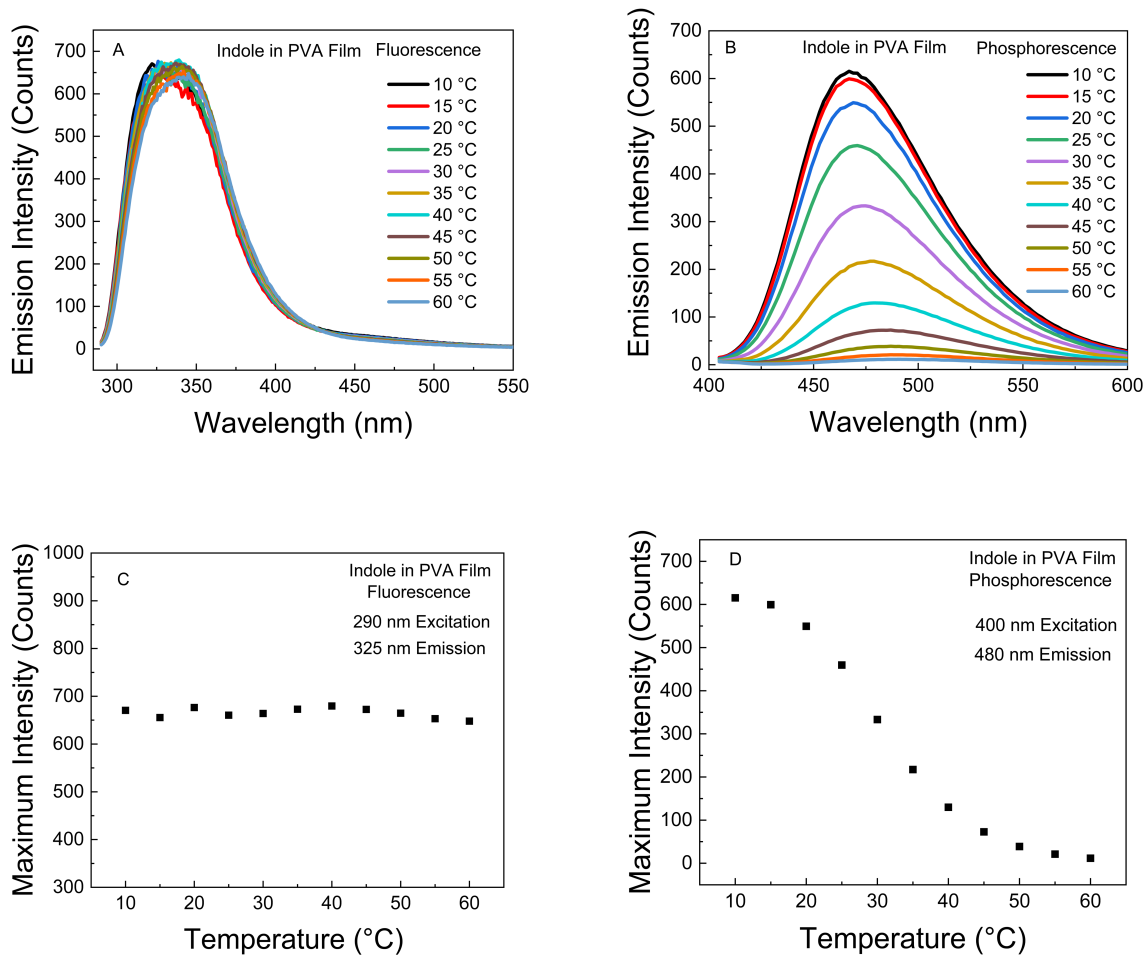
Figure 29. (A, B) Fluorescence spectra of indole in PVA film at different temperatures and fluorescence intensities of indole (at 320 nm) in PVA film as a function of temperature. (C, D) Phosphorescence spectra of indole in PVA film were measured at different temperatures, and phosphorescence intensities of indole (at 480 nm) in PVA film as a function of temperature.

Observing the phosphorescence emission on Figure 29, B the maximum peak of emission at 480 nm is decreasing with an increasing temperature. The many-fold decrease in intensity is evident when the phosphorescence maximum intensitiy at 480 nm emission are plotted versus temperature from 10 °C to 60 °C in Figure 29 (D). Similar temperature dependence has also been observed for UV (290 nm) excited phosphorescence. In conclusion, the phosphorescence of

indole in PVA film is significantly more sensitive to temperature than fluorescence. The rapid thermal deactivation of the triplet state is a known phenomenon [30,31].

3.2 2-Phenylindole Results

2-Phenylindole was the second indole derivative chosen out of the set. This particular indole derivative has a benzene ring covalently bound to the second carbon of the indole system. It was theorized that the benzene ring could increase the probability of the intersystem crossing rate occurring when using UV excitation. To begin the 2-Phenylindole system embedded in PVA, the fluorescence properties of absorption, emission, and lifetime were measured.

3.2.1 Fluorescence Properties

3.2.1.a Spectra

Absorption and fluorescence spectra of 2PI in PVA film are presented in Figure 30. The fluorescence spectrum centered around 375 nm shows a distinctive structure.
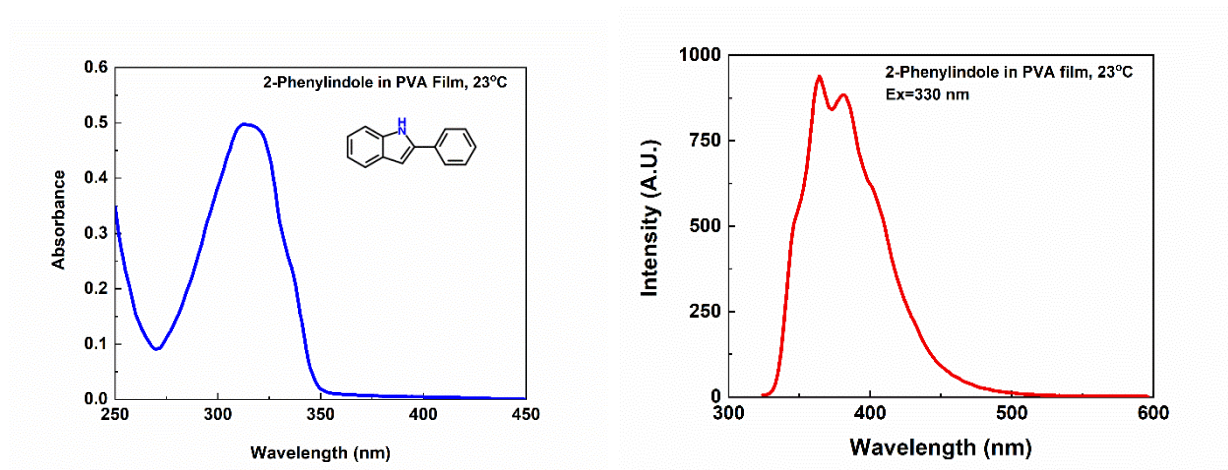
Figure 30. Absorption (left) and fluorescence (right) spectra of 2PI in PVA film.

The brightness of the 2PI in PVA film fluorescence was high, and the fluorescence background from the PVA film (blank film) was negligible. A quantum yield measurement was done to see how bright this film was to satisfy this curiosity.

3.2.1.b Quantum Yield

To measure the quantum yield of 2PI (film's brightness), we compared it with a 1 mm path length acidic solution of quinine sulfate (in 1M H_2SO_4), the best-known quantum yield standard, see Figure 31. The concentration of quinine sulfate was adjusted to yield the same absorption as 2PI in PVA film at 328 nm. With identical absorptions for reference and sample, the quantum yield of 2PI in PVA film can be calculated from the simplified expression (37):

$$Q(2PI) = Q_R \frac{I}{I_R} \frac{n^2}{n_R^2} \tag{37}$$

The spectra of 2PI in PVA film and quinine sulfate solution, measured in the same conditions, are presented in Figure 31. The quantum yield of 2PI in PVA, calculated according to the equation above, is 0.36.
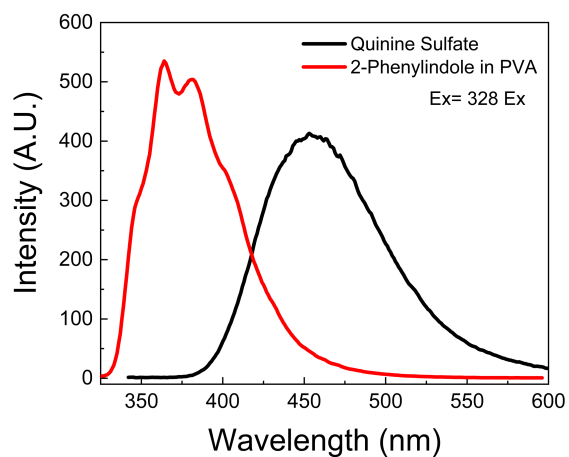
Figure 31. Fluorescence spectra of 2PI in PVA film and reference quinine sulfate in 1M H₂SO₄
were measured at 328 nm excitation, where the absorptions of both compounds are equal. These
emission spectra were used to calculate the quantum yield of 2PI.

3.2.1.c Fluorescence Lifetime

Fluorescence intensity decay of 2PI in PVA film is mono-exponential and can be a satisfactorily

fit with a single exponent lifetime of 2.1 ns, see Figure 32.
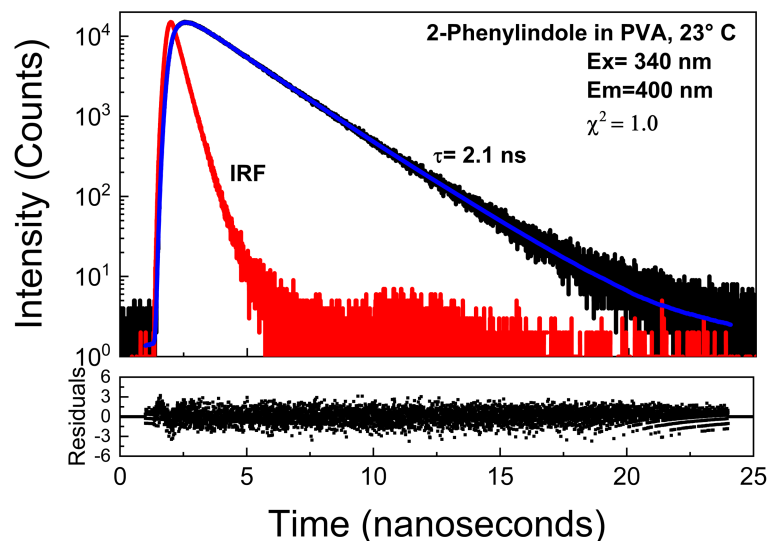
Figure 32. Fluorescence intensity decay of 2PI in PVA film. The excitation was from a pulsed UV (340 nm) LED.

The fluorescence anisotropy of 2PI in PVA film has not been reported. This measurement provides a nice representation of how high typical fluorescence anisotropy is measured.

3.2.1.d Fluorescence Anisotropy

Fluorescence anisotropy of 2PI in PVA film was measured on the Varian Eclipse using front-face configuration. G-factor corrected polarized components of 2PI in PVA fluorescence are shown in Figure 33. The "VV" spectrum is taken with a vertically oriented polarizer for both excitations and the emission. In contrast, the "VH" spectrum has a vertically oriented polarizer on the excitation and a horizontally oriented polarizer on the emission. There is a considerable difference in the vertical and horizontal components resulting in anisotropy of about 0.3, as seen in Figure 34.
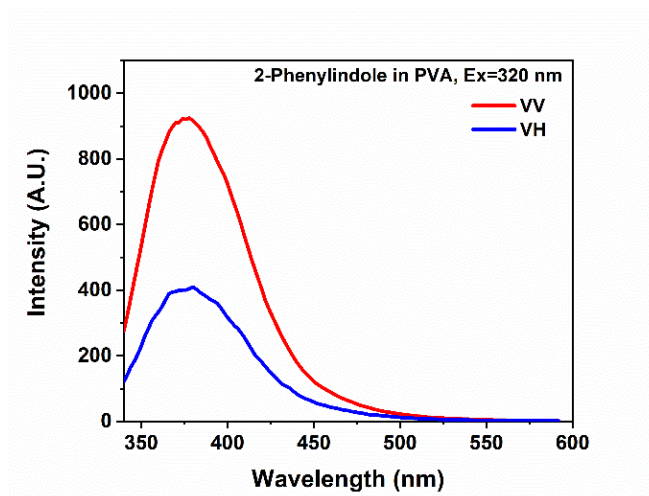
Figure 33. Polarized components of 2PI fluorescence in PVA film.
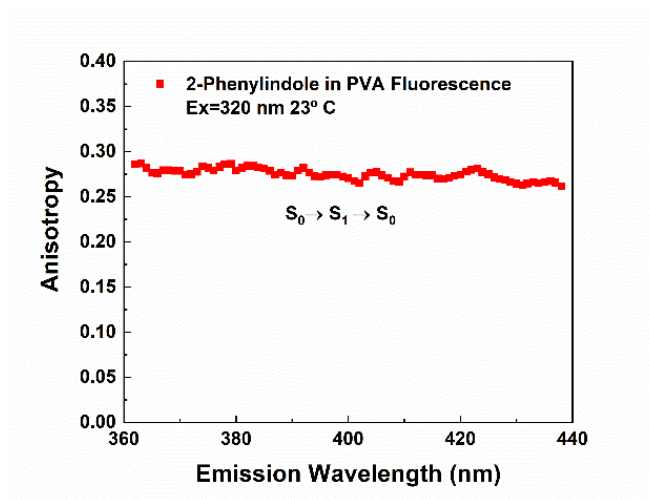
Figure 34. Fluorescence emission anisotropy of 2PI in PVA film.

3.2.2 Phosphorescence Properties

We measured the phosphorescence spectra, anisotropy, and lifetimes using normal singlet state excitation ($S_0 \rightarrow S_1$). Then, we checked the possibility of phosphorescence excitation using long-wavelength excitation (405 nm) far off the expected absorption spectrum.

3.2.2.a Phosphorescence Spectra

We excited 2PI in PVA film at 320 nm, near the absorption maximum, and observed emission in the phosphorescence mode. Then, we used 405 nm excitation outside the absorption between 275 nm and 350 nm, figure 30 left, and repeated the measurement. To our surprise, the phosphorescence spectrum, with a brightness comparable to UV excitation, could be recorded. As seen in Figure 35, both 2PI in PVA phosphorescence spectra, with UV and violet excitations, are similar, with their maxima at about 500 nm. Notably, the delayed fluorescence component seen at 340-400 nm emission when the triplet state is being excited is much weaker.
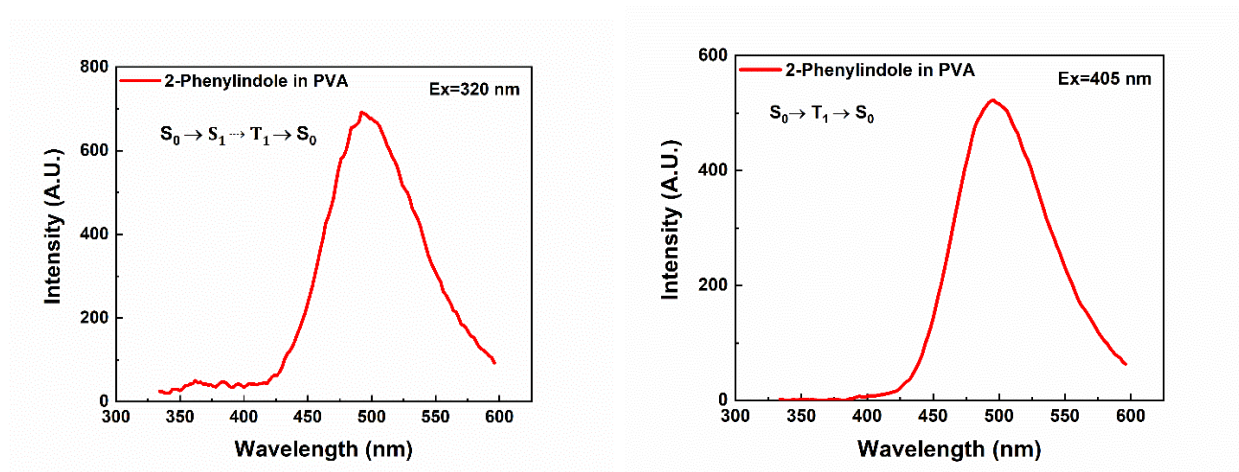
Figure 35. Phosphorescence of 2PI in PVA film with 320 nm (left) and 405 nm (right) excitations.

3.2.2.b Phosphorescence Emission Anisotropy

Next, we compared emission anisotropies of 2PI phosphorescence with 320 nm and 405 nm excitations. From the G-factor corrected polarized components (Figure 36), it is immediately apparent that their anisotropies are significantly different.
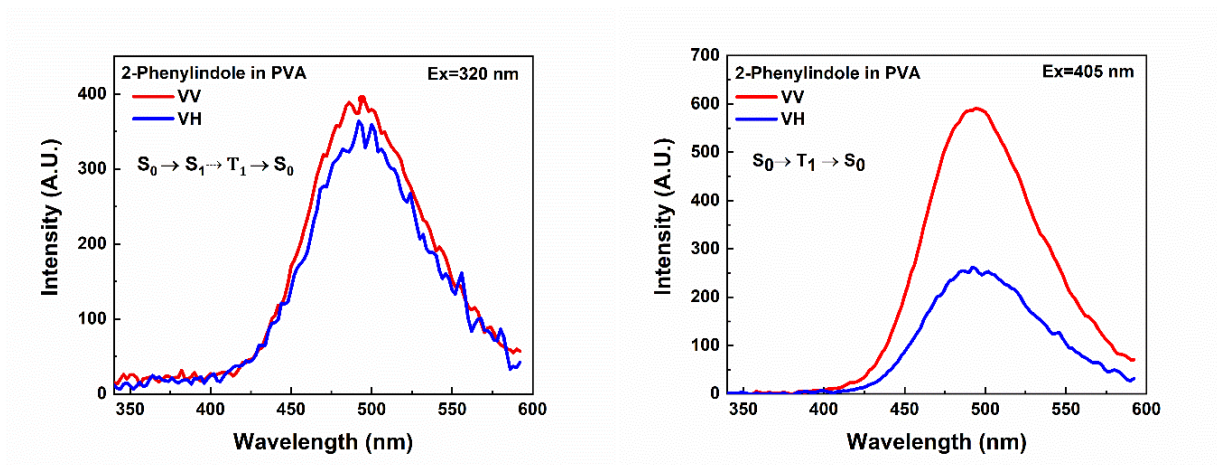
Figure 36. Polarized components of 2PI phosphorescence in PVA film with 320 nm (left) and 405 nm (right) excitations.

As shown in Figure 37, the anisotropy with UV excitation is very low when calculated. In contrast, with 405 nm excitation, the emission anisotropy is high and comparable to the earlier measured fluorescence anisotropy presented in Figure 34.
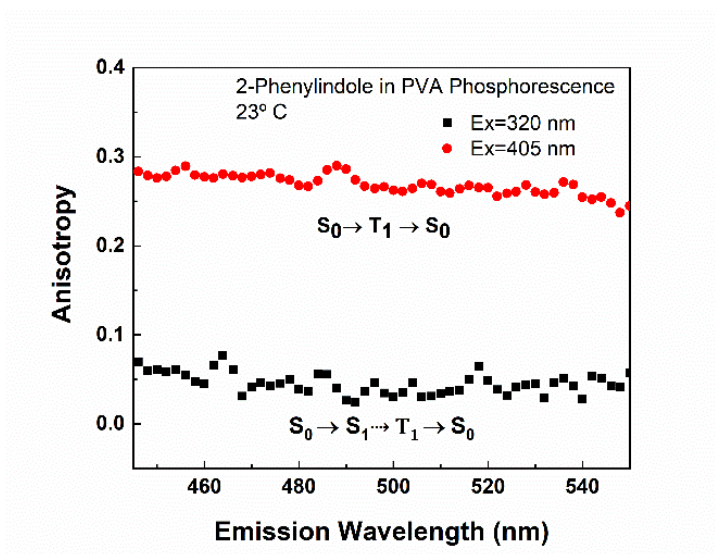
Figure 37. Phosphorescence anisotropies of 2PI in PVA film at 320 nm and 405 nm excitations.

3.2.2.c Phosphorescence Excitation Spectrum and Excitation Anisotropy

Next, we set the observation at 490 nm, near the phosphorescence maximum, and scanned the phosphorescence excitation spectrum. Figure 38 shows the measured (uncorrected for lamp intensity) excitation spectrum of 2PI in PVA film.
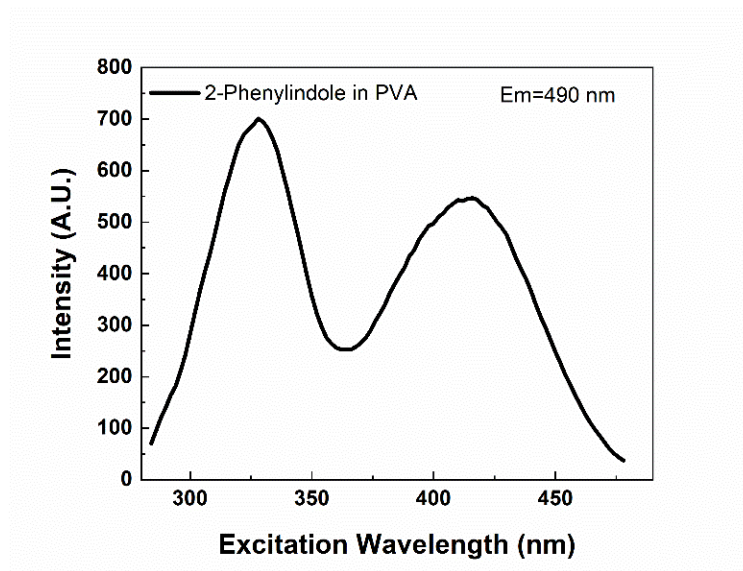
Figure 38. The phosphorescence excitation spectrum of 2PI in PVA film at 490 nm observation.

Next, we measured the polarized components of the excitation spectrum and calculated the excitation anisotropy. We used the G-factor for the 490 nm observation to calculate the anisotropy. It is important to note that for calculating the actual excitation anisotropy, there is no need for lamp correction. In Figure 39, we present the excitation anisotropy. The phosphorescence excitation anisotropy for short-wavelength excitation, below 330 nm is very low and quickly increases to values above 0.3, which was close to that measured for fluorescence anisotropy.
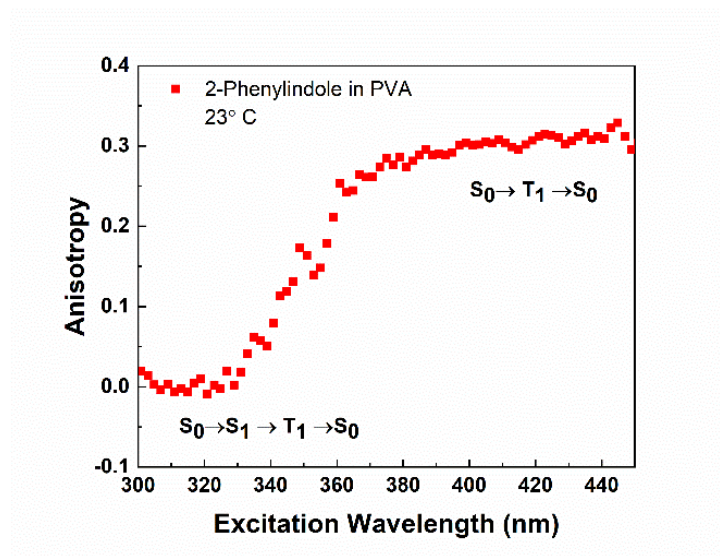
Figure 39. Phosphorescence excitation anisotropy of 2PI in PVA film at 490 nm observation.

It has been known for a long time that PVA matrices limit oxygen diffusion and provide strong stabilization of the triplet state, leading to a highly efficient phosphorescence of various compounds [24, 25, 28 42]. Nevertheless, we were initially surprised to observe that a long-wavelength excitation above the typical absorption band (>380 nm) leads to a significant phosphorescence. There is an indication that it can stimulate the spin-forbidden transition from the ground state (absorption process). However, the expected probability for such a process is very low. For this initial report, we selected 2PI because of its unusually efficient phosphorescence in a PVA film. Also, the bandwith of 2PI are at longer wavelengths when compared to 5-Bromoindole, indole, and Tryptophan. PVA presents a small absorption below 400 nm with a maximum of about 278 nm. Longer wavelength absorption of 2PI limits the amount of polymer excitation and potential excitation energy transfer from the polymer matrix to the dye. Detecting a high phosphorescence anisotropy with 405 nm excitation was crucial to eliminate such a possibility since a single-step energy transfer in isotropic media would significantly lower the observed anisotropy.

3.2.2.d Phosphorescence Lifetimes
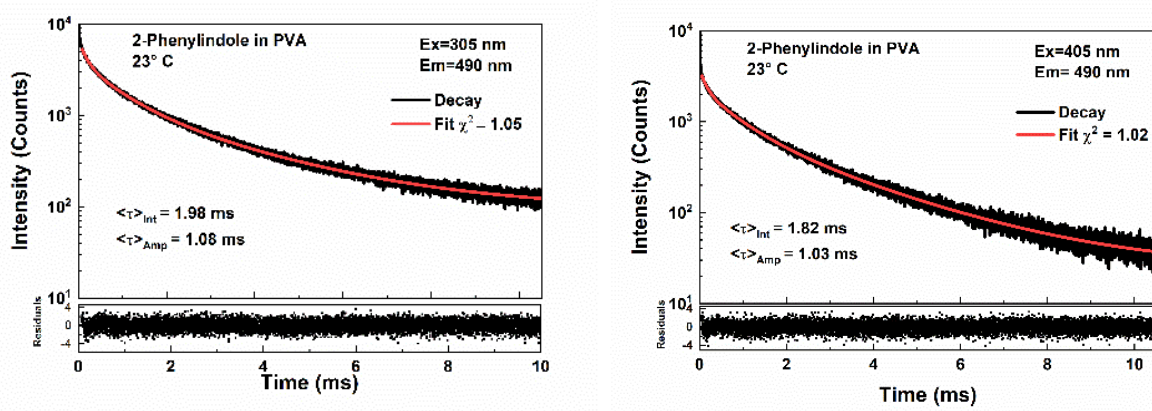
Figure 40. Phosphorescence intensity decays of 2PI in PVA at 305 nm and 405 nm excitations.

We measured phosphorescence lifetimes of 2PI in PVA film in a front-face configuration using

two excitations, 305 nm and 405 nm. Intensity decays and recovered phosphorescence lifetimes

are shown in Figure 40 and Table 2. The $<\tau>_{Int}$ and $<\tau>_{Amp}$ were calculated according to

equations 19 and 20, respectively. As expected, the recovered phosphorescence lifetimes are

similar, showing three-lifetime components. Average lifetimes for both excitations are practically

identical within the experimental error.

Excitation	τ_1 (ms)	α_1	τ_2 (ms)	α_2	τ_3 (ms)	α_3	$<\tau>_{Int}$ (ms)	$<\tau>_{Amp}$ (ms)	χ^2
305 nm	2.73±0.05	1296±6	0.82±0.04	2249±21	0.16±0.02	1683±70	1.98	1.08	1.05
405 nm	2.45±0.06	853±5	0.77±0.05	1346±16	0.14±0.03	980±58	1.82	1.03	1.02

Table 2. The lifetime component fits for 2PI in PVA film with 305 nm and 405 nm excitation.

In contrast to fluorescence, 2PI phosphorescence shows complex decays with UV and blue

excitations. In a long-lived triplet state, there are more possibilities for the interactions of 2PI

molecules with the polymer matrix, which can result in a deviation from mono-exponential

decay. We believe that oxygen quenching, although greatly limited in PVA, is responsible for

non-exponential phosphorescence decay

This additional phosphorescence observation for indole suggests that such direct triplet state excitation might be possible for tryptophan and other proteins containing tryptophan. Such a possibility would critically impact potential studies of large protein complexes. Protein solutions are pratically transparent when long wavelengths (over 400 nm) interact and provides only minimal background. In water solution at room temperature, the phosphorescence lifetime will be much shorter but still much longer than its fluorescence lifetime, thus allowing the study of slower dynamic processes of macromolecular ensembles. In addition, the phosphorescence lifetime is very sensitive to temperature and oxygen concentration.

3.3 5-Bromoindole Results

5-Bromoindole is the third set of indole derivatives being studied. There is a heavy atom, bromide, for this indole derivative, attached to the 5th carbon on the indole system. The reason 5-Bromoindole was chosen is to observe the heavy atom effect. The heavy atom effect can also increase the probability of achieving phosphorescence when exciting in the UV.

3.3.1 Absorption

The absorptions of both 5-BrI and indole in PVA film at 20^0C are shown in Figure 41. Included in Figure 41 are the chemical structures for both 5-BrI and indole. The absorption maxima for indole and 5-BrI in PVA film are 280 nm and 290 nm, respectively. The absorptions of the indole and 5-BrI agrees with previously published values [9, 88]. Absorption of 5-BrI is about twice as strong and slightly red-shifted as the indole's absorption due to the presence of the bromide ion.
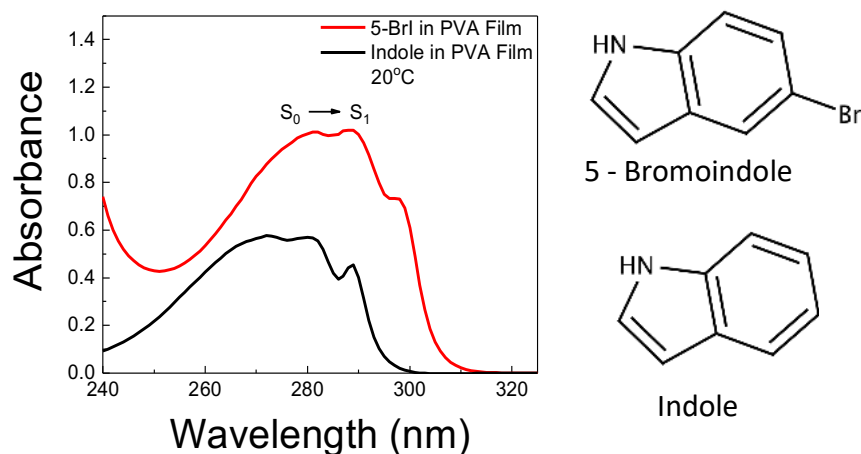
Figure 41. Absorption spectra of 5-Bromoindole and indole in PVA films. The thicknesses of the films were about 0.3 mm. The measurements were done with a reference baseline of PVA film (alone, no 5-BrI). The chemical structures of both fluorophores are on the right.

3.3.2 Fluorescence Spectra and Lifetime

Fluorescence spectra of indole and 5-BrI in PVA films were measured in front-face configuration with the excitation at 290 nm. There is a dramatic difference in their brightness. While indole has a very strong fluorescence emission, 5-BrI has an extremely weak emission. In Figure 42, we used two different intensity scales. The right (red) scale for 5-BrI is 25-fold, showing that the brightness of 5-BrI is about 50 times weaker than indole. It is not surprising because heavy atoms like bromine or iodine are efficient fluorescence quenchers [1, 2, 3]. However, the positions of fluorescence spectra are almost identical, centered at 325 nm, in contrast to the absorption spectra, see Figure 42. Using these absorption and fluorescence measurements of 5-BrI and indole (Figures 41 and 42), we estimated the quantum yield of 5-BrI in PVA film to be 0.0034, which is about two orders of magnitude smaller than the quantum yield of indole (0.35).
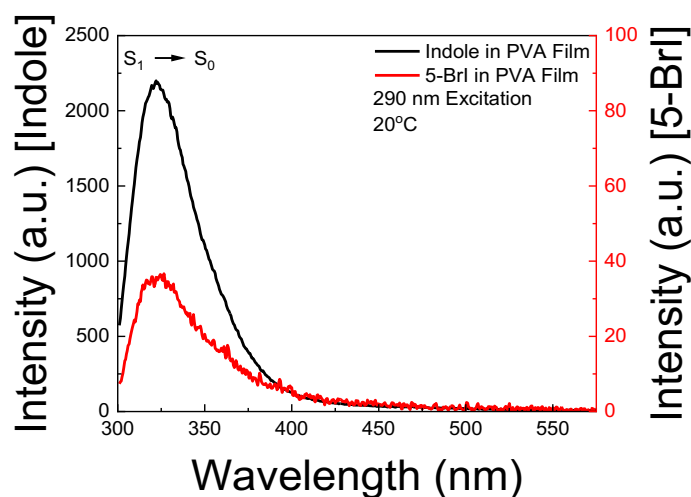
Figure 42. Fluorescence spectra of 5-Bromoindole and indole [34] in PVA films. The excitation was 290 nm.

Next, we measured the fluorescence intensity decay of 5-BrI in PVA film (Figure 43). The decay is heterogeneous, with an amplitude averaged lifetime of about 0.6 ns. This is about 8 times shorter than the indole lifetime. However, the lifetime shortening is much smaller than the change observed in the intensity measurements. We believe that extremely short components in 5-BrI intensity decay could not be seen/resolved with relatively long (0.6 ns) LED pulses. The effect is similar to a partial static quenching where part of the excited molecule is rapidly deactivated, decreasing the excited state population. Furthermore, the fluorescence decay's observation wavelength is set to 350 nm instead of the maximum emission peak at 325 nm to avoid leaking the LED excitation light and Raman scattering.
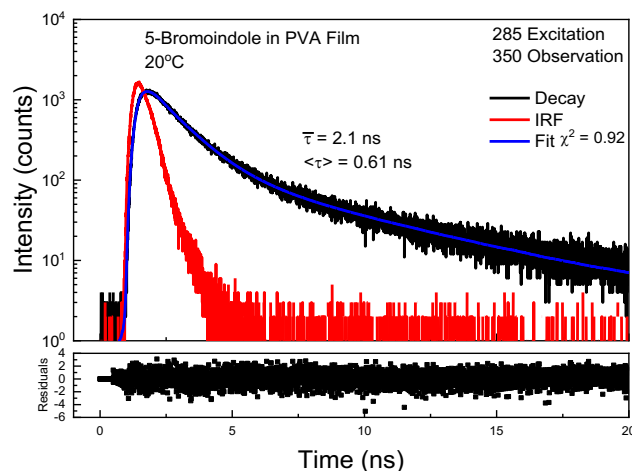
Figure 43. Fluorescence intensity decay of 5-BrI in PVA film. The excitation was 285 nm from a pulsed LED, and the observation was set to 350 nm. The decay can be satisfactorily fitted (blue line) with three exponents: α_1: 0.64 & τ_1: 0.13 ns; α_2: 0.322 & τ_2: 1.08 ns; α_3: 0.038 & τ_3: 4.9 ns.

Several of our studies' reported that indole might show phosphorescence under certain conditions. Room-temperature measurements of phosphorescence need careful oxygen removal in solutions. Indole derivatives in a solid phase on paper substrates show long-wavelength emission attributed to phosphorescence, as described in the Introduction. Long-wavelength emission of 5-substituted electro-polymerized indoles has also been reported [64]. PVA polymer is a dense matrix that significantly reduces the diffusion of oxygen. This increases fluorescence and highly enhances the phosphorescence of dyes embedded in PVA films. However, previous phosphorescence measurements were done only with the excitations to the singlet (allowed) states. Also, earlier singlet-triplet absorption measurements for various molecules were largely unsuccessful [35-37]. It should be noted that despite a lack of direct absorption measurements, an elegant method to decipher the photophysics of the triplet state has been proposed [22, 32, 33, 35, 36, 37].

3.3.3 Phosphorescence Spectra

We used the phosphorescence mode of the Varian Cary Eclipse Spectrofluorometer that can effectively gate out fluorescence. We measured the phosphorescence spectrum of 5-BrI in PVA film at 290 nm excitation, see Figure 44. First, in contrast to the fluorescence (Figure 42), the phosphorescence intensity of 5-BrI is roughly comparable to indole. Second, the 5-BrI phosphorescence spectrum is red-shifted by about 50 nm compared to the indole spectrum. These two facts suggest that the bromide atom enhances spin-orbit coupling allowing efficient intersystem crossing transition followed by phosphorescence [66, 67]. Also, the triplet state energy in 5-BrI is significantly lowered by the presence of the heavy atom.
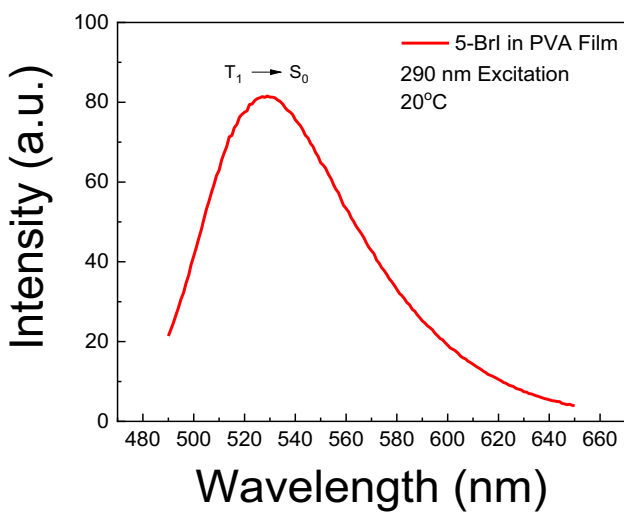
Figure 44. Phosphorescence spectrum of 5-BrI in PVA film. The excitation was 290 nm. Detection parameters were: Total decay time: 0.01s; Number of flashes: 5; Delay: 0.1ms; Gate: 5.00ms.

Next, we used long-wavelength excitation at 470 nm. Surprisingly, the phosphorescence is much stronger (about 8-fold, compared to intensity scales) than UV excitation, see Figure 45. Intrigued by this outcome, we measured the phosphorescence excitation spectrum of 5-BrI in PVA film, as

shown in Figure 46. Indeed, the phosphorescence of 5-BrI can be effectively excited up to 520 nm, with the maximum at about 475 nm. We believe the range over 350 nm for the excitation spectrum corresponds to a direct triplet state excitation ($S_0 \rightarrow T_1$); below 350 nm we have a combination of a direct triplet state excitation and singlet state excitation and intersystem crossing to the triplet state T_1.
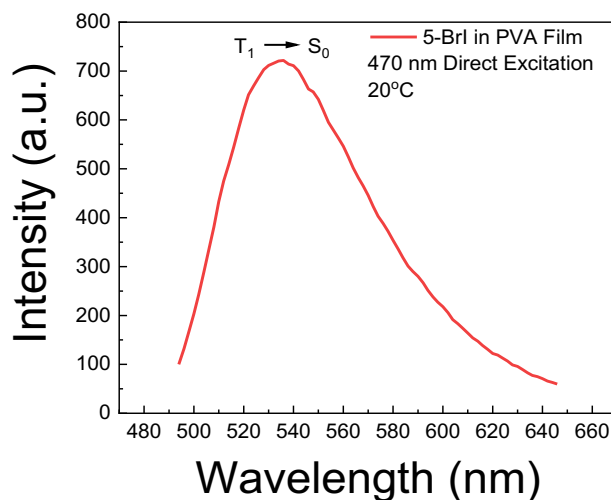
Figure 45. Phosphorescence spectrum of 5-BrI in PVA film. The excitation was 470 nm. Detection parameters were: Total decay time: 0.01s; Number of flashes: 5; Delay: 0.1ms; Gate: 5.00ms.
Such efficient direct excitation of 5-BrI in PVA film to the triplet state is another manifestation of a spin-orbit coupling. Additional measurements of lifetime and phosphorescence anisotropy were conducted to further confirm this.
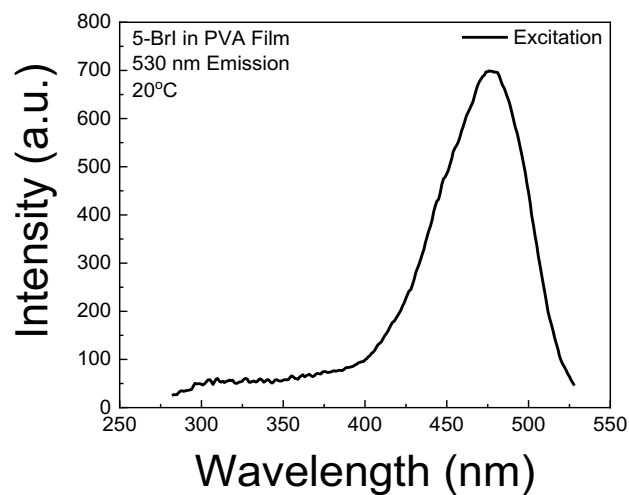
Figure 46. The excitation spectrum of 5-BrI in PVA film was observed at 530 nm. Detection parameters were: Total decay time: 0.01 s; Number of flashes: 5; Delay: 0.1 ms; Gate: 5.00 ms.

3.3.4 Phosphorescence Lifetime

The phosphorescence intensity decay of 5-BrI in PVA film with the 470 nm pulsed excitation is presented in Figure 47.
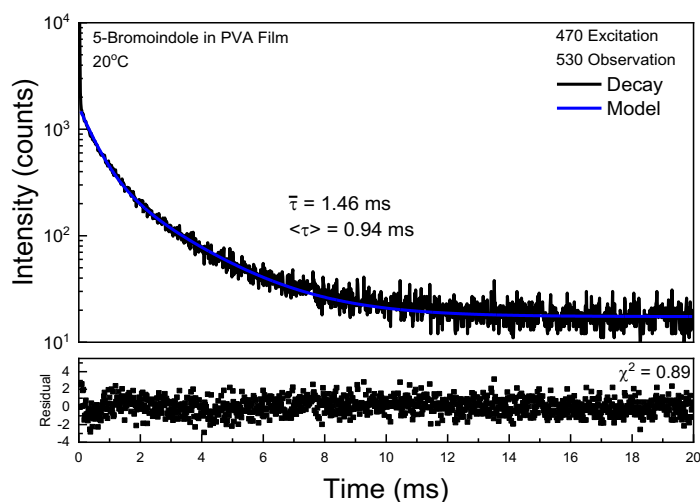
Figure 47. Phosphorescence intensity decay of 5-BrI in PVA Film with 470 nm pulsed (50Hz) excitation and 530 nm observation. The decay was fitted to 2 exponents: α_1: 0.74 τ_1: 0.53 ms; α_2: 0.26 τ_2: 2.1 ms.

The average intensity lifetime was 1.46 ms and the amplitude averaged lifetime was 0.94 ms, slightly shorter than the phosphorescence lifetime of 2-Phenylindole and indole in PVA film [8, 9].

3.3.5 Phosphorescence Anisotropy

The steady-state excitation and emission phosphorescence anisotropies of 5-BrI are shown in Figure 48. The excitation phosphorescence anisotropy shows an interesting wavelength dependence, see Figure 48, left. At shorter wavelengths, the anisotropy is low within the $S_0 - S_1$ transition, close to zero. The weak phosphorescence signal results in rather noisy anisotropy values. It is not surprising because low and negative phosphorescence anisotropies were already observed for indole and 2-Phenylinole with UV excitation [8, 9, 28]. At longer wavelengths, within the $S_0 - T_1$ transition, the anisotropy increases to a value of about 0.2.
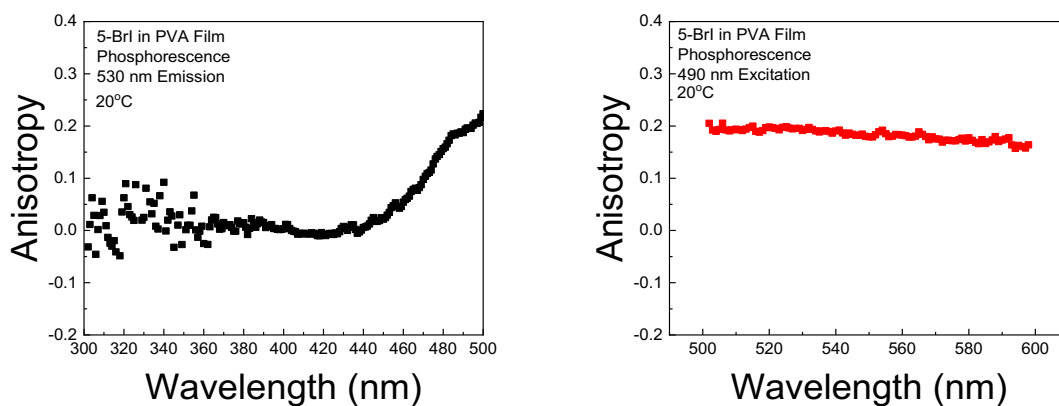
Figure 48. Phosphorescence excitation (left) and emission (right) anisotropy spectra of 5-BrI in PVA film.

The phosphorescence emission anisotropy of 5-BrI in PVA film with 490 nm excitation has a constant value of roughly 0.2 in the phosphorescence range, see Figure 48, right.

3.3.6 Temperature Dependence of Phosphorescence

We expect to see a very strong temperature dependence of phosphorescence [8, 9, 32, 33, 65]. The 5-BrI phosphorescence dramatically depends on temperature (Figure 49 A and B), in contrast to fluorescence (Figure 49 C and D), which weakly changes in this temperature region.
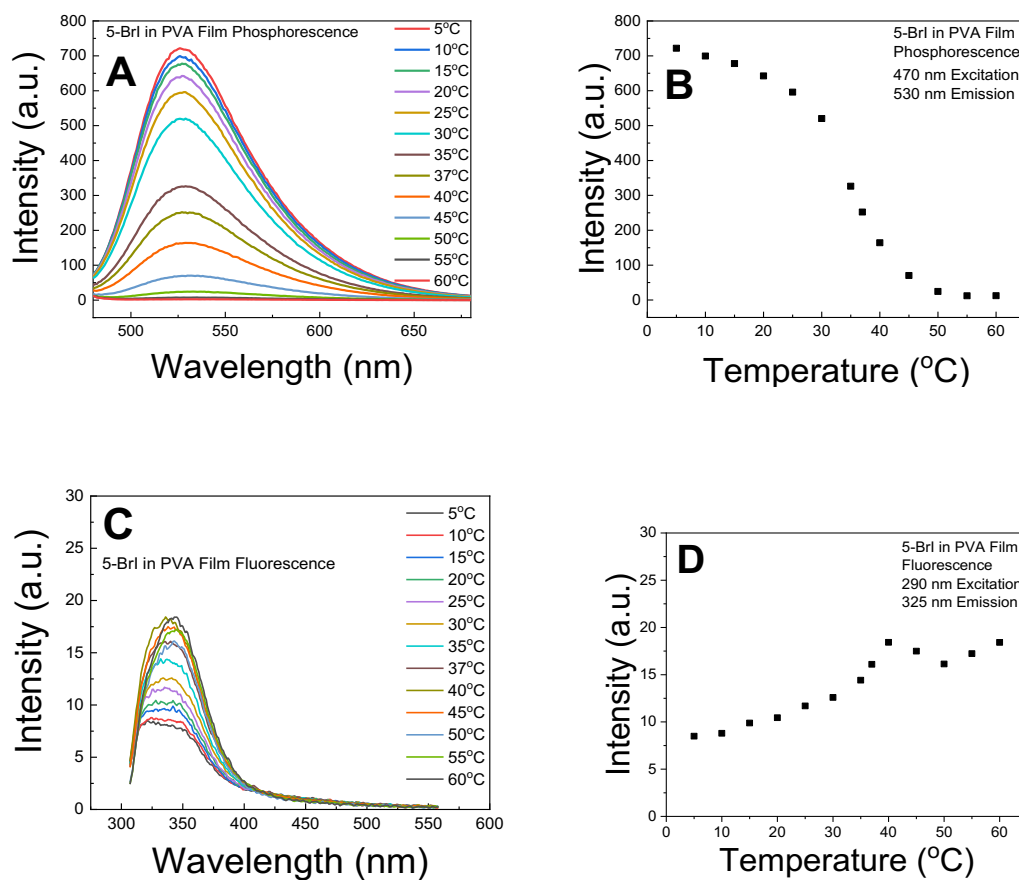
Figure 49. Temperature dependence of the 5-BrI in PVA film phosphorescence (A and B) and fluorescence (C and D). The spectra as measured with phosphorescence A and fluorescence C. Maximum intensities of phosphorescence B and fluorescence D.

Such phosphorescence temperature-dependence can be easily used for convenient temperature sensing from 20°C – 50°C, see Figure 49, A. The combination of 5-BrI in a PVA film strip with a temperature-insensitive emission sample offers a ratiometric method for temperature sensing.

3.3.7 Triplet Absorption & Quantum Yield

Relatively strong phosphorescence emission of 5-BrI PVA films with long-wavelength excitation is intriguing and inspired us to look once again into absorption in the extended wavelength range. Looking back at the absorption of 5-BrI in PVA (Figure 41), it is evident that the absorbance in

the UV dominates the measured spectrum. We remeasured the absorption at longer wavelengths and carefully subtracted the PVA alone background as described in [8], see Figure 50. There is a clear evidence of an additional peak centered at about 470 nm. We believe this peak is due to the singlet to direct triplet absorption. The absorbance at 470 nm is measurable and was found to be about 800 fold weaker than the UV (280 nm), allowing absorption to the S_1 state, see Figure 41. We want to stress that this is quite a surprise that the forbidden $S_0 \rightarrow T_1$ absorption transition can be so strong. We expect this is due to the rigid environment of the polymer matrix.
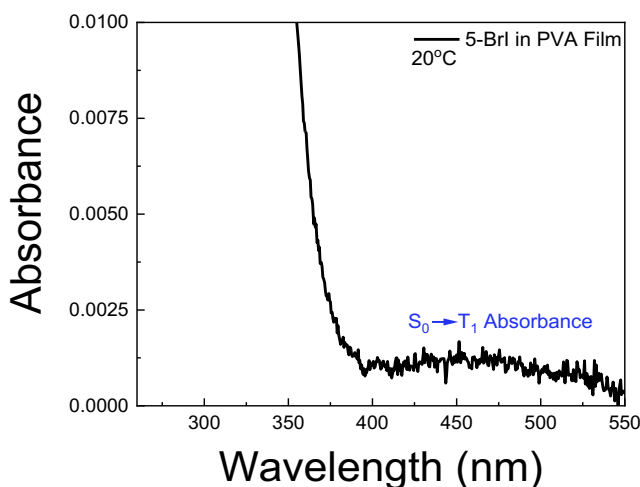
Figure 50. The absorption spectrum of 5-BrI in PVA film in the long-wavelength range.

The clear presence of the $S_0 - T_1$ transition inspired us to try the measurement at 470 nm excitation in the fluorescence mode (without gating). This measurement required the support of a 470 nm band-pass filter on the excitation path to eliminate a leak of the excitation. We were pleasantly surprised because the emission centered at 535 nm can be recorded, see Figure 51. We compared this emission with a diluted solution of Rhodamine 6G in ethanol, which was placed in a 1 mm cuvette. With these measurements, a calculation of the quantum yield for 5-BrI in PVA film was conducted using the respective absorbances at 470 nm.
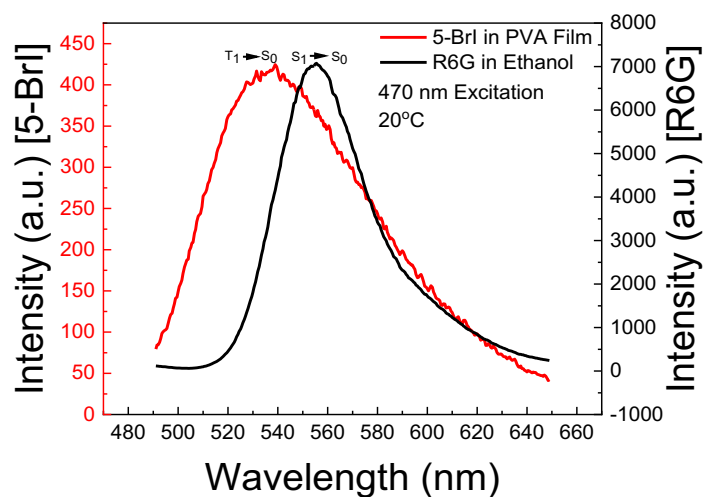
Figure 51. Phosphorescence spectrum of 5-BrI in PVA film measured in fluorescence mode (without gating) with 470 nm excitation and fluorescence spectrum of Rhodamine 6G in ethanol (in a 1 mm cuvette) measured in the same conditions. At 470 nm, the absorbance was: 0.00123 for 5-BrI in PVA film and 0.00022 for R6G in ethanol.

The calculations show that the quantum yield of 5-BrI in PVA film at 20°C is about 0.02. We want to stress that the obtained quantum yield was found by the lack of a precise $S_0 - T_1$ absorption measurement. However, we believe that this is an important finding because the possession of the quantum yields and lifetimes of both fluorescence and phosphorescence allows one, for the first time to calculate deactivation rates for the excited states (fluorescence and phosphorescence). With the addition of the phosphorescence excitation spectrum, we have the unique possibility to estimate the intersystem crossing rate from S_1 to T_1. Since quantum yields and lifetimes of phosphorescence are given by [1, 2, 63]

$$QY_F = \frac{\Gamma_F}{\Gamma_F + k_{nr}^F + k_{ISC}},\qquad(37)$$

and

$$\tau_F = \frac{1}{\Gamma_F + k_{nr}^F + k_{ISC}};\tag{38}$$

and similarly for phosphorescence

$$QY_P = \frac{\Gamma_P}{\Gamma_P + k_{nr}^P},\tag{39}$$

and

$$\tau_P = \frac{1}{\Gamma_P + k_{nr}^P}.\tag{40}$$

We can directly calculate radiative rates for fluorescence and phosphorescence as

$$\Gamma_F = \frac{QY_F}{\tau_F},\tag{41}$$

and

$$\Gamma_P = \frac{QY_P}{\tau_P}.\tag{42}$$

With the present experimental results, we cannot separate the non-radiative rate and intersystem crossing rate, and we can only calculate a cumulative non-radiative deactivation rate for an excited singlet state

$$k_{nr} = k_{nr}^F + k_{ISC} = \frac{1 - \Gamma_F \ \tau_F}{\tau_F},\tag{43}$$

and for phosphorescence

$$k_{nr}^P = \frac{1 - \Gamma_P \ \tau_P}{\tau_P}.\tag{44}$$

At this point, we can only estimate the value of the intersystem crossing rate using the phosphorescence excitation spectrum shown in Figure 46. At the wavelength 470 nm, we only have a direct T_1 excitation. At wavelengths below 320 nm, the triplet state population is due to

71

singlet excitation and intersystem crossing and some contribution from the direct higher triplet state excitation. Assuming that at 290 nm, we dominantly excite the singlet state, we can calculate that the intersystem crossing rate, k_{ISC} is

$$k_{ISC} \leq \frac{(1-10^{-OD_{470}})P_{290}}{(1-10^{-OD_{290}})P_{470}},$$

(45)

Where OD_{290}, and OD_{470} are absorptions measured at 290 nm and 470 nm, P_{290} and P_{470} are the phosphorescence signal measured with 290 nm excitation and 470 nm excitation, respectively.

Table 3 presents all the estimated molecular photophysical parameters associated with 5-BrI excited states' deactivation.

	Fluorescence (s⁻¹)	Phosphorescence (s⁻¹)
Γ	$5.57*10^6 \pm 0.02$	$2.12*10^1 \pm 0.02$
k_{nr}	$1.63*10^9 \pm 0.02$	$10.42*10^2 \pm 0.02$
k_{ISC}	$\leq 2.2*10^{-4} \pm 0.1$	

Table 3. Photophysical rate constants of 5-BrI in PVA

Again to further emphasize the values calculated for fluorescence and phosphorescence radiative rates (Γ) they were obtained via the quantum yield and lifetimes (equations 41 and 42 respectively). This shows that 5-BrI is heavily quenched from the bromide since the fluorescence nonradiative rate (k_{nr}) is fairly dominate when compared to fluorescence radiative rate Γ. However looking at the phosphorescence radiative rate it is just under one order of magnitude compared to the phosphorescence nonradiative rate. The low difference in the phosphorescence radiative and nonradiative rates shows that phosphorescence emission has a higher probability of occurring. For k_{ISC} it is typically a low probability transition and the rate shows to be roughly in the 10^{-4} inverse seconds range. Fluorescence and as well as the nonradiative processes in fluorescence will be the dominate pathways for 5-BrI.

3.4 Tryptophan Results

As of now, the photoluminescent properties of the indole derivatives have been studied. It has been shown a longer wavelength of excitation can be used to observe phosphorescence emission. The longer wavelength (direct excitation) also shows to have high excitation anisotropy; consequently, it produces a high emission anisotropy. The phosphorescence lifetimes are comparable when excited through UV and the direct excitation wavelength. Furthermore, the phosphorescence emission with a temperature change behaves as typical phosphorescence. Now all of the information known from the indole derivatives will be applied to the amino acid residue tryptophan.

3.4.1 Absorption and Fluorescence

Our first attempts at RTP measurements of TRP in PVA film have shown that the detected intensity signals are relatively weak. We compared the fluorescence/phosphorescence of TRP and indole. The samples (doped PVA films) were prepared with approximately the same concentrations of both compounds of about 7 mM. The RTP measurements with UV (285 nm) excitation were possible for indole and TRP films and revealed similar intensities. However, the long-wavelength excitation at 410 nm gave different results. We realized that RTP measurements of TRP from a single PVA film with long-wavelength excitation require some alteration when using commercial spectrofluorometers. We prepared a series of TRP-doped PVA films with a slightly higher concentration of about 10 mM. The absorption and fluorescence spectra did not show any concentration effect, and spectral profiles were identical to spectra measured from low-concentration films, as seen in Figures 52 and 53.
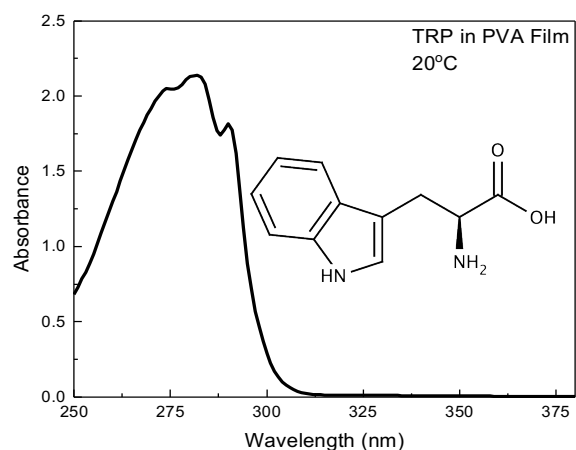
Figure 52. The absorption spectrum of tryptophan in PVA film. A chemical insert is shown in the graph.
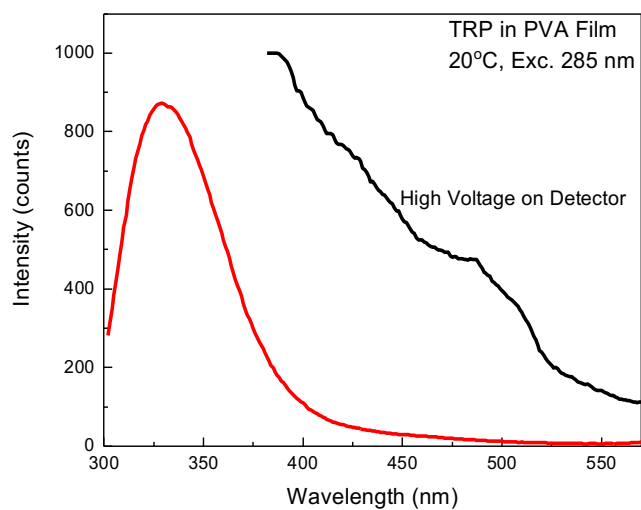
Figure 53. Fluorescence spectrum of tryptophan in PVA film. The insert shows the long-wavelength tail of the spectrum measured at a higher voltage on the detector.

Figure 52 shows the measured absorption spectrum of TRP in PVA film after removing the residual PVA background. The excitation wavelength chosen for the fluorescence emission was 285 nm. The fluorescence emission intensity spectra have a strong signal between 300 and 400

nm. The fluorescence spectrum of TRP in PVA film shows a minor irregularity in the long-wavelength tail at about 450 - 500 nm, see Figure 53. A higher voltage is applied, and a long-wavelength tail of the fluorescence spectrum is shown in Figure 53 (black line). The increased voltage emphasized the irregularity. The irregularity shows the phosphorescence emission emanating from the steady state fluorescence measurements. We used multiple TRP-doped PVA films for the RTP study with long-wavelength excitation (direct triplet state excitation).

3.4.2 Phosphorescence Emission

The PVA films are inert in non-polar solvents, and these solvents were used as index matching fluids. The PVA film in the presence of such solvents becomes invisible, and all reflections are eliminated. We cut the TRP-doped PVA film into 1 cm x 4 cm strips and packed them into a 4 mm x 10 mm quartz cuvette. Next, the cuvette was filled with the index-matching fluid (mixture of benzene – n-heptane, 1:1) and then sealed. We used this cuvette with multiple films for RTP measurements with long-wavelength excitation at 410 nm. We used the convenient square geometry configuration for these measurements with a 4 mm path facing the detector. The measurements with UV excitation were done using a single film and front-face configuration, which was necessary to avoid a residual PVA absorption. RTP spectra from TRP-doped PVA are shown in Figure 54.
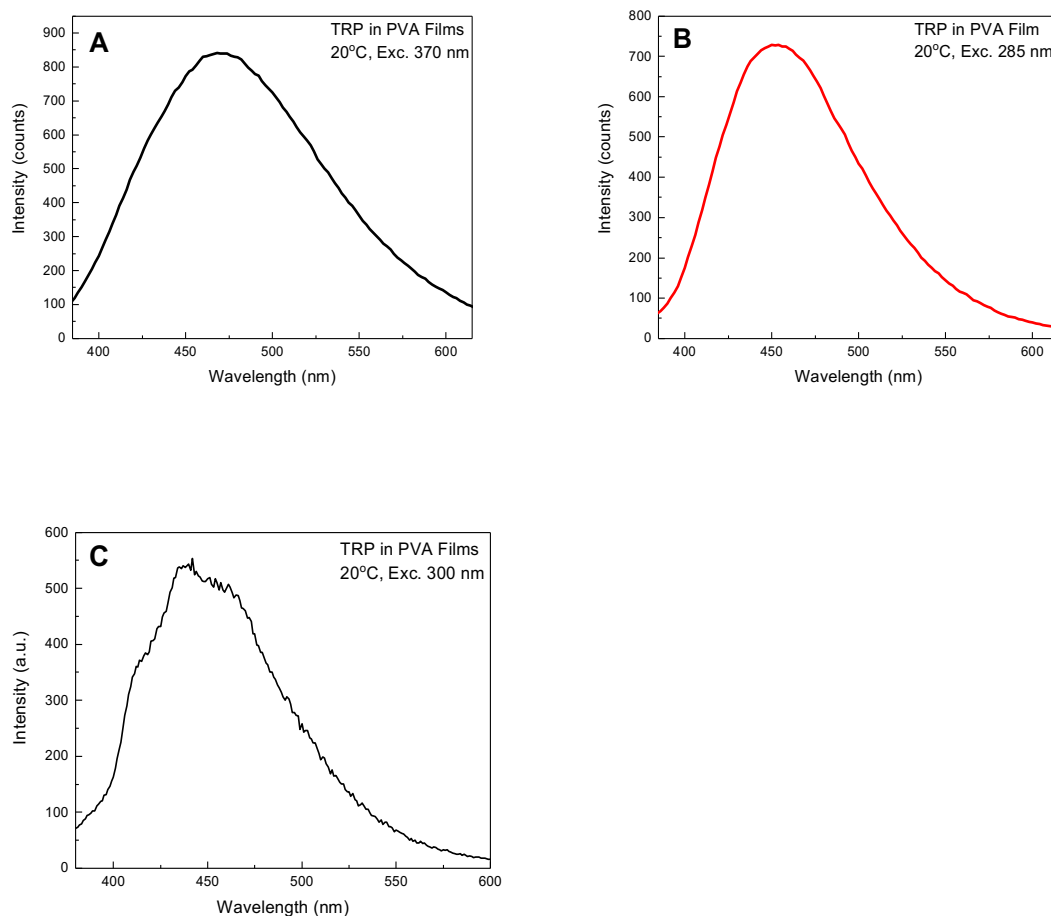
Figure 54. A: Phosphorescence spectrum of tryptophan in PVA film measured with long-wavelength excitation, 370 nm, far from absorption. B: Phosphorescence spectrum of tryptophan in PVA films measured with UV excitation. C: Phosphorescence emission with lower emission slits to emphasize the structure. The parameters in phosphorescence measurements were: Total Decay Time: 0.050 seconds, Number of Flashes: 5, Delay Time: 0.100 milliseconds, and Gate Time: 5.00 milliseconds.

The measurements were done in the same observation conditions, with lower voltage on the detector for UV excitation. The spectrum with long-wavelength excitation is slightly shifted towards longer wavelengths, similarly to indole [9]. Figure 3C shows the phosphorescence spectrum measured with smaller (5 nm) slits, with higher voltage on the detector, and without smoothing. This slightly structured spectrum looks very similar to the spectrum measured by Horie

and Vanderkooi for a protein containing tryptophan [72]. The large slits (20 nm) are responsible for the lack of structures in spectra presented in Figures 54A and 54B.

3.4.3 Phosphorescence Excitation, Emission, and Anisotropy

Next, we measured the excitation spectrum. The RTP excitation spectrum of TRP (measured for multiple films) is shown in Figure 55. The observation was set at 500 nm, and the excitation was scanned from 280 nm to 480 nm.
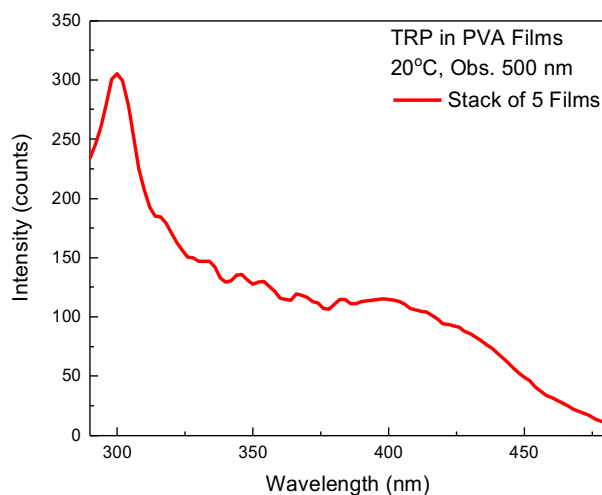
Figure 55. The phosphorescence excitation spectrum of tryptophan in PVA films with observation at 500 nm. The parameters in phosphorescence measurements were the same as in Figure 54.

There is clear evidence for long-wavelength absorption at around 350-450 nm; a more efficient excitation is in the UV region. In the long-wavelength region, the most efficient excitation is around 400 nm. Suppose the long-wavelength absorption of TRP is responsible for the direct excitation to the triplet state. In that case, the phosphorescence anisotropy should be different (higher) than UV excitation, which involves the singlet excited state. Therefore, we measured the RTP excitation anisotropy of TRP-doped PVA films over the entire wavelength scale, as seen in Figure 56.
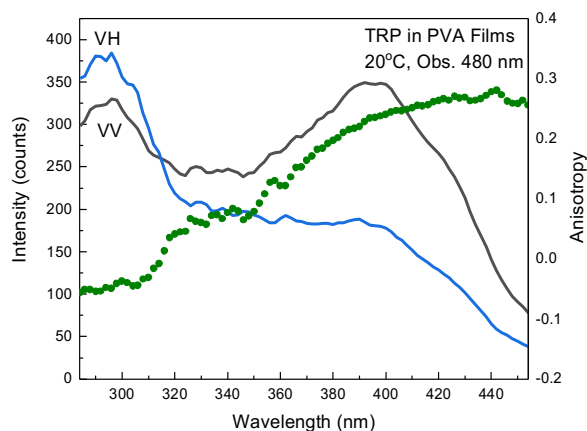
Figure 56. Phosphorescence excitation anisotropy (shown as green dots) spectrum of tryptophan in PVA films. The intensity polarization component VH is shown in blue, and the VV polarization component is in black.

The observation wavelength was set to 480 nm (near the maximum emission in Figure 54), then VV and VH polarization excitation spectra were measured. Excitation anisotropy was calculated as a function of wavelength with equation 25. In fact, in the UV region, the anisotropy (green dots) is negative, while in the long-wavelength region, it is positive, reaching almost a value of 0.3. The higher anisotropy values signify that the molecules are populating to a specific state, i.e., the phosphorescence state (wavelengths 470-570 nm). For the emission anisotropy measurements, we selected 425 nm for the excitation. The emission RTP anisotropy spectrum (Figure 57) is high across the emission spectrum, only slightly depending on the observation (emission) wavelength.
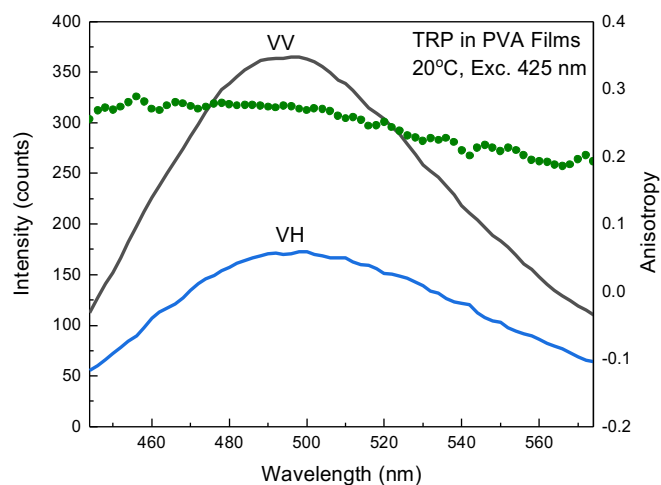
Figure 57. Phosphorescence emission anisotropy (shown as green dots) spectrum of tryptophan in PVA films. VV emission spectra in black, and VH emission spectra in blue.

3.4.4 Phosphorescence and Fluorescence Temperature Dependence

Phosphorescence is known for its strong dependence on temperature [21, 32, 33, 65, 71]. Since the typical phosphorescence lifetime is in the order of microseconds – seconds, it is susceptible to environmental factors (e.g., quenching). The temperature-dependent RTP of TRP-doped PVA films with long-wavelength excitation is shown in Figure 58A. Clearly, at 50-60^{0}C, the phosphorescence is already below the measurement capability. Figure 59 shows a similar yet slightly steeper dependence for UV excitation. Both cases of temperature dependences (excitation 410 nm and 285 nm) show that TRP in PVA film could be a possible temperature sensor.

In Figure 58B, the intensity values (read at the peak) are normalized (divided by the max value at 5°C.). The temperature measurements began at 5°C, where the phosphorescence intensity was the greatest, and cooling to 5°C favors the phosphorescence radiative rate. As temperature increases, the phosphorescence emission intensity begins to decrease. Hence, the non-radiative rate will now

out-compete the radiative rate. Also, as a consequence of the increased molecular relaxation (due to polymer viscosity change), there is a slight spectral red shift in Figures 58A (410 nm excitation) and 59A (285 nm excitation) as temperature increases.
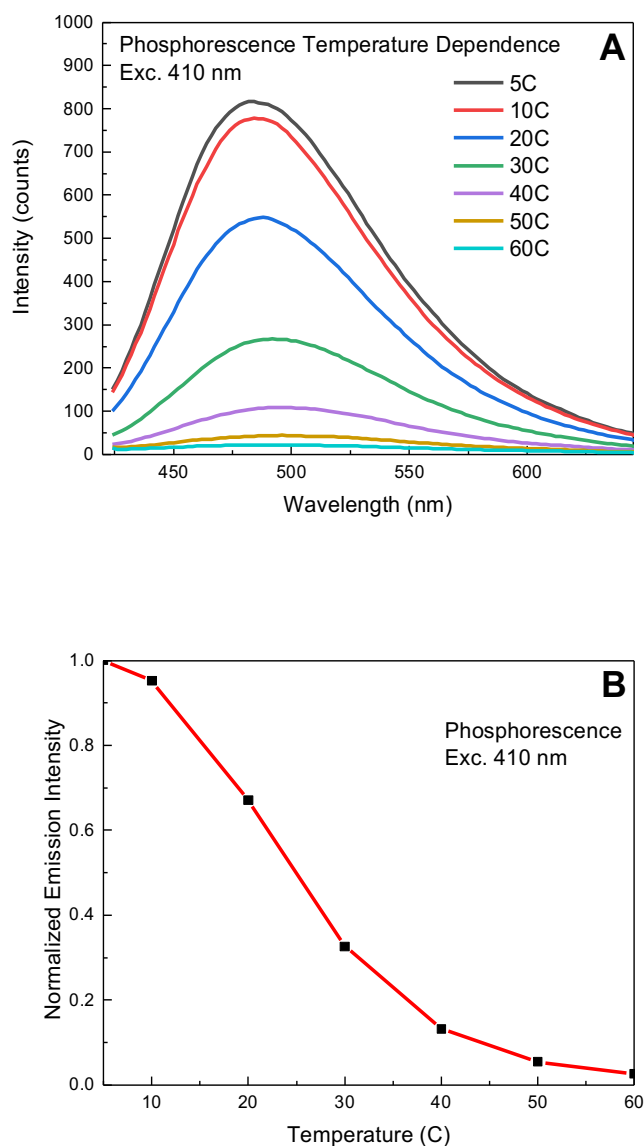
Figure 58. Temperature dependence of tryptophan in PVA films phosphorescence at long-wavelength excitation (A). On B, it shows the maximum intensity value as a function of temperature at 5^0C. Normalization was done with the maximum value at 5^0C.
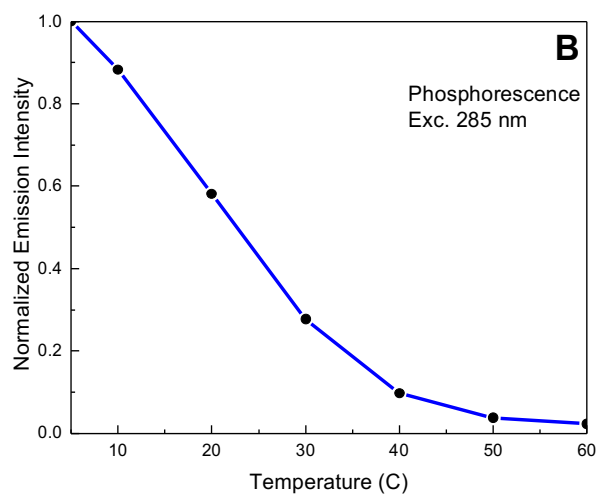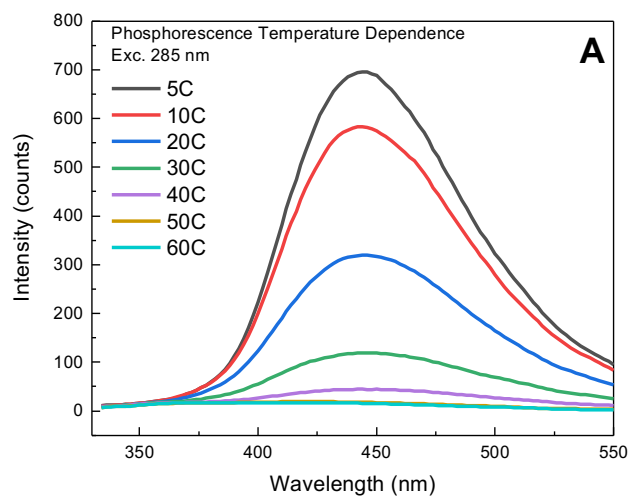
Figure 59. Temperature dependence of tryptophan in PVA films phosphorescence at UV excitation (A). On B, it shows the maximum intensity value as a function of temperature. Normalization was done with the maximum value at 5^0C.

Subsequently, we measured fluorescence dependence on temperature, see Figure 60A. At 60°C, fluorescence intensity decreases to about 50% (Figure 60B), which is different from the indole

film, where a very weak dependence was observed [4]. The fluorescence does not drastically decrease as a function of temperature compared to the similar phosphorescence measurements.
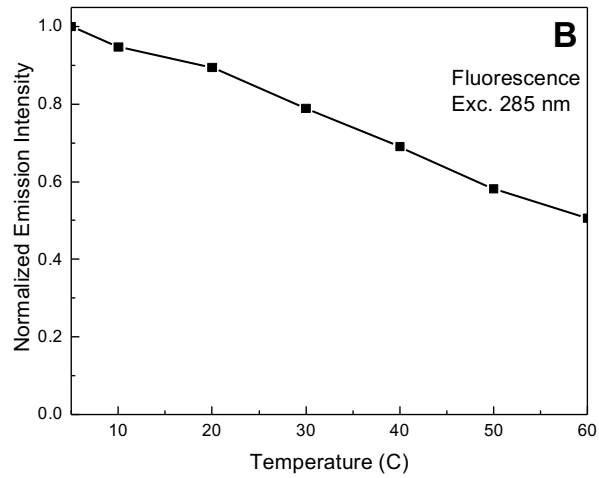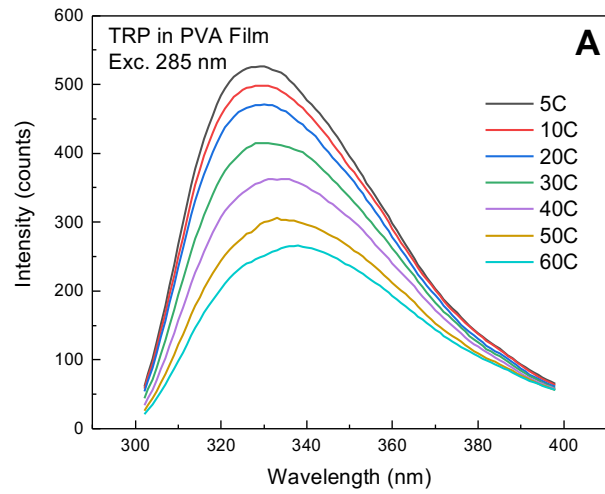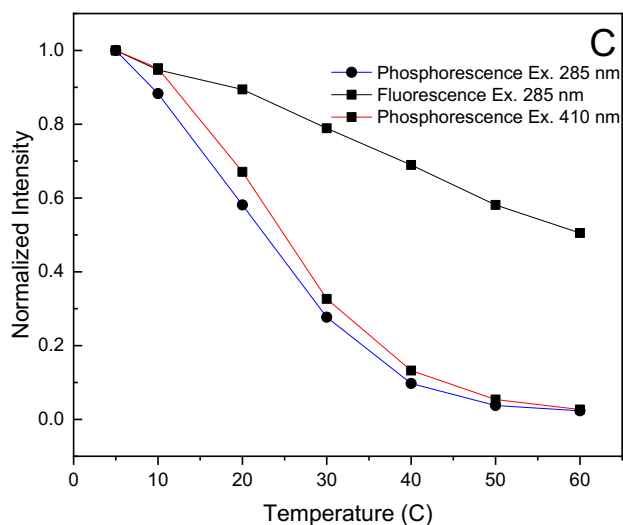
Figure 60. Temperature dependence of tryptophan in PVA films fluorescence at UV-wavelength excitation (A). On B, it shows the maximum emission intensity value normalized at 5^0C. On C, all temperature dependences of phosphorescence (excitation 285 nm and 410 nm) as well as fluorescence with an excitation of 285 nm are shown together for comparison.

The phosphorescence temperature dependencies differ slightly for UV and long-wavelength excitations. Such temperature dependence may seem puzzling at first glance. However, it should be noted that UV excitation results in the population of the S_1 state, and a different deactivation path from the singlet excited state (non-radiative transition S_1-S_0) contributes to the total deactivation. As a result, fewer molecules appear in the triplet state, which is responsible for phosphorescence. This deactivation path (S_1-S_0) is not present with the direct long-wavelength excitation.

3.4.5 Phosphorescence Lifetime

Finally, we measured the lifetime of RTP of TRP-doped PVA films with long-wavelength and UV excitation, see Figure 61. The lifetime is heterogeneous, with an average value of sub-milliseconds for direct (A) and UV (B). (see also Table 4), which is a few times shorter than indole [9].
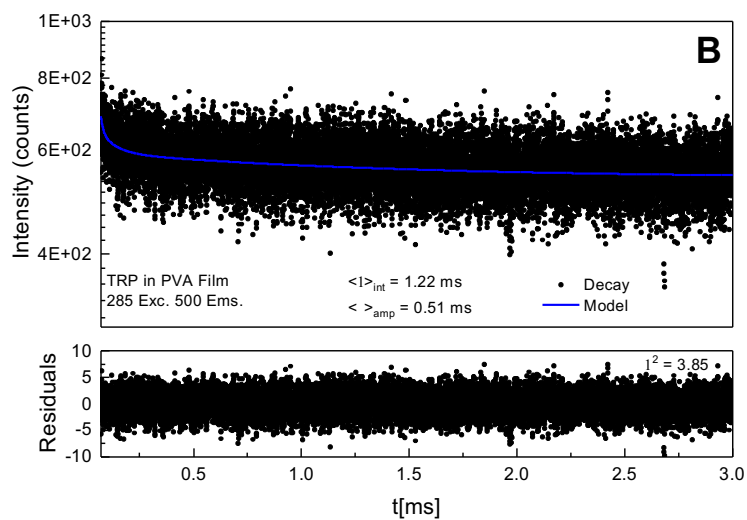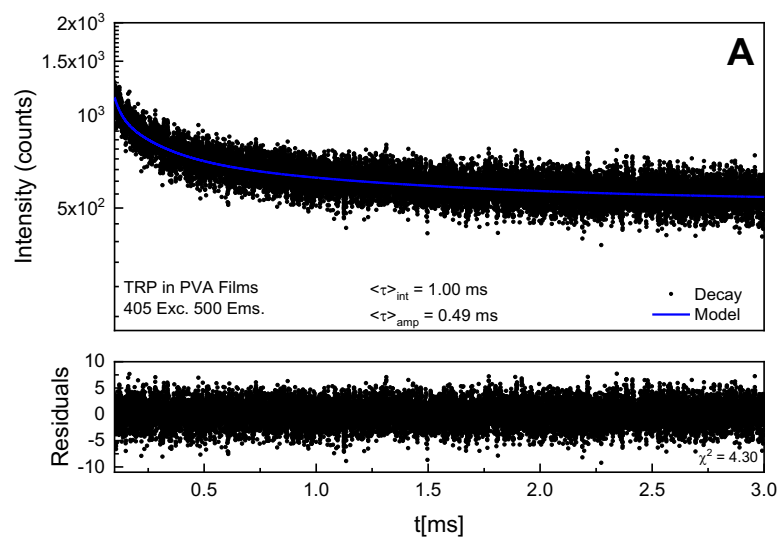
Figure 61. Phosphorescence lifetime of tryptophan in PVA films with long-wavelength excitation (A). UV excitation with the same observation was conducted (B).

	405 nm Excitation	285 nm Excitation
α_1 (counts):	221.4±21.3	56.5±16.9
τ_1 (milliseconds):	1.18 ± 0.14	1.29 ± 0.47
α_2 (counts):	260.1±59.8	49.4±75.0
τ_2 (milliseconds):	0.18 ± 0.05	0.07 ± 0.15
α_3 (counts):	136±163	43.4±197
τ_3 (milliseconds):	0.03 ± 0.04	0.01 ± 0.07
$<\tau>_{int}$ (milliseconds):	1.00	1.22
$<\tau>_{amp}$ (milliseconds):	0.49	0.51

Table 4. Intensity and amplitude average lifetimes with their components fitting to three exponentials. Excitation was 405 nm, and emission was observed at 500 nm (Left). The right shows the components when the excitation was set to 285 nm and the observation was set to 500 nm.

The lifetime of TRP in PVA film was excited at 405 nm and 285 nm using the FT300's flash lamp set at 300 Hz. The observation wavelength was set to 500 nm, close to the maximum phosphorescence intensity. The lifetime was fitted to 3 components. All components are in the millisecond-submillisecond range with a dominant (42%) of 0.18 ms for direct excitation. As for UV excitation, the dominant component is 1.29 ms (38%). The average lifetime is in the millisecond/submillisecond range. The lifetime of TRP moiety in proteins depends on the exposure to the aqueous phase and varies from tens of microseconds to milliseconds [21]. The short lifetime of TRP fluorescence can be used only to study the fast motions of the molecule itself or short peptide chains. The longer phosphorescence lifetime enables monitoring motions of whole proteins and their domains. A high limiting phosphorescence anisotropy makes this possible for time-resolved studies in the submillisecond range.

Chapter 4 Conclusions

4.1 Indole

The possibility of direct triplet excitation of indole followed by phosphorescence is highly unexpected. We repeated the PVA film preparation, spectroscopic measurements, and indole purification multiple times. The results are very much reproducible, and measurements can be performed at room temperature using any commercial spectrofluorometer with a phosphorescence function.

One could ask if the observed directly excited phosphorescence is specific to PVA. We prepared PMMA (Poly (methyl Methacrylate)) films with indole to answer this question. The phosphorescence spectrum with blue excitation is presented in Figure 23, bottom. Compared to the spectrum in PVA (Figure 23, black line), the spectrum in PMMA is slightly shifted towards shorter wavelengths. We believe this is a result of the slightly lower polarity of PMMA. PMMA was used to show an example that not only PVA can be used to observe direct triplet excitation of indole.

Another question one could ask is - is there a possibility to determine the kinetic parameters of the photo-processes involved in indole phosphorescence/fluorescence? To describe the photo-processes occurring with UV and blue excitations, we need to consider: (1) non-radiative and (2) radiative transitions from S_1 to S_0, (3) intersystem crossing from S_1 to T_1, (4) non-radiative and (5) radiative transitions from T_1 to S_0. We currently have only three independent measurements: the fluorescence lifetime and quantum yield and the phosphorescence lifetime of. The two remaining parameters involving the triplet state can only be estimated. An attempt was made by Kearns and co-workers [35-37]. They used phosphorescence excitation spectra and proposed to

estimate a ratio of intersystem crossing efficiency (Φ_{ISC}) to singlet-triplet extinction coefficient (ε_{ST}). In this case, the dependence will have the form

$$\frac{\Phi_{ISC}}{\varepsilon_{ST}} = \frac{P(290)}{P(405)}\frac{I(405)}{I(290)}\frac{1}{\varepsilon_{SS}},$$

(46)

where P(290) and P(405) are phosphorescence intensities with UV and blue excitation, (ε_{SS}) is the extinction coefficient of indole UV absorption, and I(290) and I(405) are intensities of the excitation light. When using the Varian Eclipse spectrofluorometer, the excitation intensities are normalized with a reference photodetector, and the equation further simplifies.

What are some possible applications of indole phosphorescence excited directly with blue light? First, measurements used within the visible spectral region are incomparably easier than in the UV region and do not require special optics. Second, the unwanted background from the solvent/medium is much smaller with blue light excitation than with UV. Third, the directly excited phosphorescence anisotropy is positive and high, whereas it is negative and small with UV excitation. This allows one to study large protein rotational motions using time-resolved phosphorescence (anisotropy decays) of tryptophan. Many other applications of this phenomenon are possible, like temperature sensing or polarization-based sensing.

4.2 2-Phenylindole

We studied the fluorescence and phosphorescence properties of 2PI in PVA film at room temperature. The most important finding is the possibility of direct triplet state T_1 excitation with violet light. In contrast to conventional phosphorescence excitation via its singlet S_1, the phosphorescence anisotropy when excited directly to the T_1 state is as high as fluorescence anisotropy. The high phosphorescence anisotropy of indoles which are the side chain of the

amino acid tryptophan found in many proteins) opens new possibilities in large protein conformational studies and macromolecular dynamics occurring in the micro-millisecond time region.

It is noteworthy that the part of myosin in muscle systems responsible for rotation-causing movement [56] contains tryptophan. It is conceivable that it will be possible to excite this indole directly and thus take advantage of its high anisotropy. This may prove to be more sensitive to monitoring its angular position than the current attempts to measure the orientation by the fluorescence polarization.

4.3 5-Bromoindole

5-BrI in PVA film fluorescence at room temperature is very weak, about 50 times weaker than indole fluorescence. However, the phosphorescence of 5-BrI is only about twice as weak as indole phosphorescence with UV excitation. The phosphorescence is significantly stronger when excited at longer wavelengths. The excitation at 470 nm is about 10 times stronger than at 290 nm, as seen in Figure 46. It should be noted that the Varian spectrofluorometer is equipped with a reference photodiode and corrects for the lamp excitation power. The phosphorescence excited at longer wavelengths has high positive anisotropy, showing a lack of involvement of any intermediate state, and is very sensitive to temperature, as shown in Figure 49. We were pleasantly surprised by two facts. First, we separated direct absorption to the triplet state signal (Figure 50). Second, without gating, phosphorescence measurements were done in fluorescence mode. These two measurements allow us to estimate the phosphorescence QY directly and to decipher all photo-physical parameters involved in room temperature excited states deactivation (fluorescence and phosphorescence) of 5-BrI in PVA film. We believe this is the first successful attempt to recover complete photophysical parameters for excited states deactivation.

4.4 Tryptophan

It has been shown that it is possible to excite TRP directly to the triplet state. This excitation results in phosphorescence emission, which we believe to be an important finding. PVA and most solvents and buffers do not absorb the blue light used for the direct TRP excitation. Powerful laser light sources are readily available for excitation in this spectral range. Also, long-wavelength excitation results in lower scattering, which might be necessary in macromolecule (protein) studies. The biological background noise will be reduced as compared to typical UV excitation.

Temperature studies of TRP in PVA film show that it is indeed sensitive to different temperatures. The temperature sensitivity implies a possible application as a temperature probe. However, the essential finding is that direct excitation to the triplet state results in a high phosphorescence anisotropy of TRP. In combination with sub-millisecond phosphorescence lifetime, time-resolved phosphorescence anisotropy can be used to investigate slower rotations and motions of macromolecules and molecular ensembles. The conventional excitation of the triplet state through a single state requires UV excitation and, more importantly, results in low or negative phosphorescence anisotropies. Therefore, conventional UV excitation has never been used in time-resolved phosphorescence anisotropy measurements of proteins. The long-wavelength direct excitation opens new possibilities toward utilizing the TRP triplet state for phosphorescence anisotropy decay measurements.

4.5 Future work.

4.5.1 Why is discovering direct triplet state excitation in PVA films important for future studies?

The possibility of measuring direct triplet state excitation for proteins is an important breakthrough for studying large protein dynamics. However, the efficiency of such a process in a

liquid solution under room-temperature conditions is extremely low. In fact, nobody has ever observed such phosphorescence, although many have tried.

At this point, it is unknown exactly what enables phosphorescence in PVA films. A possible explanation is that the micro-rigidity in the film reduces oxygen diffusion, which limits oxygen quenching and thus enhances phosphorescence. In addition, some other interactions with the polymer chains might facilitate breaking the symmetry rule and allow ISC transition in the excited state and for direct triplet state excitation. This system will make it possible to initiate the search for different conditions that could perturb molecular orbitals and help break the symmetry rule. A potential possibility is an external electric or magnetic field. Another possibility is perturbation by inert (off-absorption bands) light. For example, 600 nm high-intensity light could be a factor. All these potential options can now be explored. Finding an external perturbation factor that can be independently controlled could easily facilitate any uses of directly excited phosphorescence in physiological conditions.

Bibliography

[1] Gryczynski, Z. and Gryczynski, I. Practical Fluorescence Spectroscopy. 2019. Taylor & Francis. ISBN: 9781439821695.

[2] Lakowicz, JR. Principles of Fluorescence Spectroscopy, 3rd edition. 2006. Springer. ISBN: 987-0-387-31278-1.

[3] Valeur, B. and Berberan-Santos, M. N. Molecular Fluorescence: Principles and Applications. 2012. Wiley-VCH Verlag GmbH & Co. KGaA. ISBN: 9783527328376.

[4] Jameson, D. M. Introduction to Fluorescence. 2014. CRC Press. ISBN: 9780367865702.

[5] Harris, D. C. and Bertolucci, M. D. Symmetry and Spectroscopy An Introduction to Vibrational and Electronic Spectroscopy. 1978. Oxford University Press. Inc. ISBN-13: 978-0-486-66144-5.

[6] McGlynn, S. P., Azumi, T., Kinoshita, M. Molecular Spectroscopy of the Triplet State. 1969. Prentice-Hall, Inc.

[7] Becker, W. The bh TCSPC Handbook, 7th edition. 2017.

[8] Gryczynski, Z., Kimball, J., Fudala, R., Chavez, J., Ceresa, L., Szabelski, M., Borejdo, J., Gryczynski, I. Photophysical Properties of 2-Phenylindole in Poly (vinyl alcohol) Film at Room Temperature. Enhanced Phosphorescence Anisotropy with Direct Triplet State Excitation. Methods Appl Fluoresc. 2020. 8(1):014008.

[9] Chavez, J., Ceresa, L., Kitchner, E., Kimball, J., Shtoyko, T., Fudala, R., Borejdo, J., Gryczynski, Z., Gryczynski, I. On the possibility of direct triplet state excitation of indole. JPPB:Biology. 2020. 208.

[10] Chavez, J., Kimball, J., Ceresa, L., Kitchner, E., Shtoyko, T., Fudala, R., Borejdo, J., Gryczynski, Z., Gryczynski, I. Luminescence properties of 5-Bromoindole in PVA films at room temperature: Direct triplet state excitation. Journal of Luminescence. 2021. 230.

[11] Chavez, J. L., Ceresa, L., Reeks, J. M., Strzhemechney, Y., Kimball, J., Kitchner, E., Gryczynski, Z., Gryczynski, I. Direct Excitation of Tryptophan Phosphorescence. A New Method for Triplet States Investigation. Methods Appl. Fluoresc. 2022.

[12] Saviotti, M., Galley, W. Room temperature phosphorescence and the dynamic aspects of protein structure. Proc. Natl. Acad. Sci U.S.A. 1974. 71(10):4154-4158.

[13] Mersol, J., Steel, D., Gafni, A. Detection of intermediate protein conformations by room temperature tryptophan phosphorescence spectroscopy during the denaturation of Escherichia coli alkaline phosphatase. Biophys. Chem. 1993. 48: 281-291.

[14] Gershenson, A., Schauerte, J., Giver, L., Arnold, F. Tryptophan phosphorescence study of enzyme flexibility and unfolding in laboratory-evolved thermostable esterases. 2000. Biochemistry. 39(16):4658-4665.

[15] Strambini, G., Gonelli, M. Tryptophan luminescence from liver alcohol dehydrogenase in its complexes with coenzyme. A comparative study of protein conformation in solution. Biochemistry. 1990. 29(1): 196-203.

[16] Vanderkooi, J., Calhoun, D., Englander, S. On the prevalence of room-temperature protein phosphorescence. Science. 1987. 236(4801): 568-569.

[17] Strambini, G., Cioni, P., Puntoni, A. Relationship between the conformation of glutamate dehydrogenase, the state association of its subunit, and catalytic function. Biochemistry. 1989. 28(9): 3808-3814.

[18] Papp, S., Vanderkooi, J. Tryptophan phosphorescence at room temperature as a tool to study protein structure and dynamics. Photochem. Photobiol. 1989. 49(6):775-784.

[19] Schlyer, B., Schauerte, J., Steel, D., Gafni, A. Time-resolved room temperature protein phosphorescence: nonexponential decay from single emitting tryptophans. Biophys. J. 1994. 67(3):1192-1202.

[20] Strambini, G., Gonelli, M., Galley, W. Room temperature phosphorescence of Trp-314 as monitor of subunit communication in alcohol dehydrogenase from horse liver. Biochemistry. 1990. 29(1): 203-208.

[21] Fischer, C., Gafni, A., Steel, D., Schauerte, J. The triplet-state lifetime of indole in aqueous and viscous environments: significance to the interpretation of room temperature phosphorescence in proteins. J. Am. Chem. Soc. 2002. 124(35): 10359-10366.

[22] Kowalska-Baron, A., Chan, M., Galecki K., Wysocki, S. Photophysics of indole, tryptophan and N-acetyl-l-tryptophanamide (NATA): heavy atom effect, Spectrochim. Acta A Mol. Biomol. Spectrosc. 2012. 98: 282-289.

[23] Kowalska-Baron, A., Galecki, K., Wysocki, S. Room temperature phosphorescence study on the structural flexibility of single tryptophan containing proteins. Spectrochim, Acta. A. Mol. Biomol. Spectrosc. 2015. 134: 380-387.

[24] Haustein, C., Savage, W., Ishak, C., Pflaum, R. Room-temperature phosphorescence of 3- and 5-subsituted indoles. Talanta. 1989. 36(11): 1065-1068.

[25] Kowalska, B., Choudhary, P., Montes, D. The effect of immobilization in the PVA films on the fluorescence and phosphorescence lifetime of indole and its derivatives. Food Sci. Biotechnol. 2011. 75(2): 3-14.

[26] Deribamar, J., Campiglia, A. Room temperature phosphorescence characteristics of indole-3-propionic acid, DL-indole-3-lactic acid, and indole-3-glycolic acid on low background paper substrate. Microchem. J. 1995. 52(1): 101-112.

[27] Gryczynski, Z., Kawski, A. Directions of the electronic transition moments of dioxydo-p-terphenyl. Z. Naturforsch. A. 1988. 43(3): 193-195.

[28] Kawski, A., Gryczynski, I., Gryczynski, Z. Fluorescence and phosphorescence anisotropy spectra of indole in poly (vinyl alcohol) film at room temperature. Z. Naturforsch. A. 1994. 49(11): 1091-1092.

[29] Yamashita, S., Tomita, G. The delayed fluorescence of indole in alcohol-alkane mixed glasses at 77K. Z. Naturforsch. B. 1978. 33(10): 1136-1141.

[30] Bridges, J., Williams, R. The fluorescence of indoles and aniline derivatives. Biochem. J. 1968. 107(2): 225-237.

[31] Gryczynski, I. Wiczk, W., Johnson, M., Lakowicz, J. Lifetime distributions and anisotropy decays of indole fluorescence in cyclohexane/ethanol mixtures by frequency-domain fluorometry. Biophys. Chem. 1988. 32(2-3): 173-185.

[32] Gryczynski, I., Kawski, A., Nowaczyk, K., Paszyc, S., Skalski, B. Temperature effect on the luminescence of synthetized Y_t-based in PVA film. Biochem. Res. Commun. 1981. 98(4): 1070-1075.

[33] Gryczynski, I., Kawski, A., Nowaczyk, K., Cherek, H. Thermal deactivation of the lowest singlet and triplet excited states of acridine dynes in poly(vinyl alcohol) films. 1985. J. Photochem. 31(2-3): 265-272.

[34] Byrdin, M., Duan, C., Bourgeois, D., Brettel, K. A long-lived triplet state is the entrance gateway to oxidative photochemistry in green fluorescent proteins. J. Am. Chem. Soc. 2018. 140(8): 2897-2905.

[35] Rothman, W., Case, A., Kearns, D. Determination of singlet-triplet absorption spectra from phosphorescence excitation spectra: alpha-bromonaphthalene. J. Chem. Phys. 1965. 43. 1067.

[36] Borkman, R. Kearns, D. Investigation of singlet-triplet transitions by the phosphorescence excitation method. Spectra determination of intersystem crossing quantum yield and extinction coefficients of singlet-triplet transitions. Chem. Commun. 1966. 14: 446-447.

[37] Parker, C. A. Photoluminescence of Solutions. Elsevier Publishing Company. Amsterdam-London-New York. 1968.

[38] Domanus, J., Strambini, G. B., Galley W. C. Heterogeneity in the thermally-induced quenching of the phosphorescence of multi-tryptophan proteins. Photochem. Photobiol. 1980. 31: 15-21.

[39] Kai, Y., Imakubo, K. Temperature dependence of the phosphorescence lifetimes of heterogenous tryptophan residues in globular proteins between 293 and 77 K. Photochem. Photobiol. 1979. 29: 261-265.

[40] Vanderkooi, J. M., Berger, J. W. Excited triplet states used to study biological macromolecules at room temperature. Biochimica et Biophysica Acta (BBA). 1989. 976: 1-27.

[41] Vanderkooi, J. M., Calhoun, D. B., Englander, S. W. On the prevalence of room-temperature protein phosphorescence. Science. 1987. 236: 568-569.

[42] Gryczynski, Z., Kawski, A. Substituent effects on the luminescence of 2-substitued 3-methylquinoxalines in poly (vinyl alcohol) films. Zeitschrift fur Naturforschung A. 2014. 46: 304-306.

[43] Albrecht, A. C. Polarizations and assignments of transitions: The method of photoselection. J. Mol. Spectrosc. 1961. 6: 84-108.

[44] Michl, J. Thulstrup, E. Spectroscopy with polarized light. Solute Alignment by Photoslection in Liquid Crystals, Polymers, and Membranes (New York: VCH Publisher, Inc). 1986.

[45] Lewschin, W. L. Polarisierte fluoreszenz und phosphoreszenz der farbstofflosugen. IV Z. Phys. 1925. 32: 307-326.

[46] Perrin, F. La fluorescence des solutions. Ann. Phys. 1929. 10: 169-275.

[47] Herzberg, G. Teller, E. Schwingungsstruktur der Elektronenubergange bei mehratomigen Molekulen. Z. Phys. Chem. 1933. 21B. 410.

[48] Murrell, J. N. Pople, J. A. The intensities of the symmetry-forbidden electronic bands of benzene. Proceedings of the Physical Society. Section A. 1956. 69: 245-252.

[49] Lier, A. D. Interaction of the vibrational and electronic motions in some simple conjugated hydrocarbons. Zeitschrift fur Naturforschung A. 1958. 13a: 429-438.

[50] McClure, D. S. Triplet-singlet transitions in organic molecules lifetime measurements of the triplet state. J. Chem. Phys. 1949. 17: 905-913.

[51] McClure, D. S. Spin-orbit interaction in aromatic molecules. J. Chem. Phys. 1952. 20: 682-686.

[52] Weissman, S. I. Fluorescence spectrum of triphenylmethyl at 4K. J. Chem. Phys. 1954. 22. 155.

[53] Craig, D. P., Hollas, J. M., King, G. W. Upper limit to the intensity of the 3400 A singlet-triplet absorption in benzene. J. Chem. Phys. 1958. 29. 974.

[54] King, G. W., Pinnington, E. H. The effect of oxygen on the 3400-A singlet-triplet absorption of benzene. J. Mol. Spectrosc. 1965. 15: 394-404.

[55] Eaton, D. F. Reference materials for fluorescence measurements. Pure Appl. Chem. 1988. 60: 1107-1114.

[56] Dos Remedios, C. G., Millikan, R.G., Morales, M. F. Polarization of tryptophan fluorescence from single straited muscle fibers. A molecular probe of contractile state. J. Gen. Physiol. 1972. 59: 103-120.

[57] Mazhul, V. M., Zaitseva, E. M., Shavlovsky, N. M., Stepanenko, O. V., Kuzetsova, I. M., Turoverov, K. K. Monitoring of actin unfolding by room temperature tryptophan phosphorescence. Biochemistry. 2003. 42: 13551-13557.

[58] Gonnelli, M., Strambini, G. B. Time-resolved protein phosphorescence in the stopped-flow: denaturation of horse liver alcohol dehydrogenase by urea and guanidine hydrochloride. Biochemistry. 1997. 36: 16212-16220.

[59] Strambini, G. B. Singular oxygen effects on the room-temperature phosphorescence of alcohol dehydrogenase from horse liver. Biophys. J. 1983. 43: 127-130.

[60] Strambini, G. B., Cioni, P. Pressure-temperature effects on oxygen quenching of protein phosphorescence. J. Am. Chem. Soc. 1999. 121: 8337-8344.

[61] Cioni, P. Oxygen and acrylamide quenching of protein phosphorescence correlation with protein dynamics. Biophys. Chem. 2000. 87: 15-24.

[62] Gacintov, N., Brenner, H. The triplet state as a probe of dynamics and structure in biological macromolecules. Photochem. Photobiol. 1989. 50(6): 841-858.

[63] Douglas, M., Wong, R., Seybold, P. G. Fluorescence quantum yields and their relation to lifetimes of rhodamine 6G and fluorescein in nine solvents: improved absolute standards for quantum yields. Photochem. Photobiol. 2007. 75(4): 327-334.

[64] Jennings, P., Jones, A. C., Mount, R. Fluorescence properties of electropolymerized 5-subsituted indoles in solution. J Chem. Soc. Faraday. Trans. 1998. 94: 3619-3624.

[65] Gryczynski, I., Kawski, A., Janic, I., Gryczynski, Z. Thermal deactivation of the lowest excited states of 5,6-benzoquinoline in poly (vinyl alcohol) film. Acta Phys. Pol. 1986. A70: 113-119.

[66] Borkman, R., Kearns, D. Heavy-atom and substituent effects on S-T transitions of halogenated carbonyl compounds. J. Chem. Phys. 1967. 46. 2333.

[67] Aaron, J., Spann, W., Winefordner, J. Quantitative phosphorescence study of interactions of cytosine and cytidine and its nucleotides in frozen aqueous solution. Talanta. 1973. 20(9): 855-865.

[68] Belford, G. G., Belford, R. L., Weber, G. Dynamics of fluorescence polarization in macromolecules. Proc. Natl. Acad. Sci. USA. 1972. 69: 1392-1393.

[69] Tao, T. Time-dependent fluorescence depolarization and Brownian rotational diffusion of macromolecules. Biopolymers. 1969. 8: 609-632.

[70] Kinosita, K., Kawato, S., Ikegami, A. A theory of fluorescence polarization decay in membranes. Biophys. J. 1977. 20: 289-305.

[71] Su, Y., Phua, S.Z.F., Li, Y., Zhou, X., Jana, D., Lui, G., Lim, W.Q., Ong, W.K., Yang, Ch., Zhao, Y. Ultralong room temperature phosphorescence from amorphous organic materials toward confidential information encryption and decryption. Sci. Adv. 2018. 4(5).

[72] Horie, T., Vanderkooi, J.M. Phosphorescence of tryptophan from parvalbumin and actin in liquid solution. FEBS Letters. 1982. 147.

[73] Jennings, P., Jones, A. C., Mount, A. R., Thomson, A. D. Electrooxidation of 5-subsituted indoles. J. Chem, Faraday Trans. 1997. 93(21): 3791-3797.

[74] Meng, X., Harricharran, T., Juszczak, L. J. A Spectroscopic Survey of Substituted Indoles Reveals Consequences of a Stabilized ^1L_b Transition. 2012. 89(1): 40-50.

[75] Nie, G., Zhang, Y., Xu, J., Zhang, S. Low potential facile electrosynthesis of free sanding poly(5-methyoxyindole) film with good fluorescence properties. Journal of Electroanalytical Chemistry. 2008. 662(1): 121-127.

[76] Jennings, P., Jones, A. C., Mount, A. R. Photophysics of Novel Electropolymerised Indoles. Central Laser Facility Annual Report. 1997. ISBN: 0902376802.

[77] Ozisik, H., Saglam, S., Bayari, S. H. Molecular structure and vibrational spectra of 4-, 5-, 6-chloroindole. Struct Chem. 2008. 19: 41-50.

[78] Sundaraganesan, N., Umamaheswari, H., Joshua, B. D., Meganathan, C., Ramalingam, M. Molecular structure and vibrational spectra of indole and 5-aminoindole by density functional theory and ab initio Hartree-Fock calculations. Journal of Molecular Structure. 850: 84-93.

[79] Merrer, D. C., Ozcentinkaya, S., Shinnar, A. E. Experimental and theoretical ultraviolet spectra of haloindoles. Tetrahedron Letters. 2004. 45(25): 4899-4902.

[80] Sanyal, N. K., Sriastava, S. L., Tripathi, S. R. Ultraviolet and infared spectra of substituted indoles. Spectrochimica Acta Part A: Molecular Spectroscopy. 1982. 38(8): 993-995.

[81] Rao, R., Sashidar, M. A., Rao, S. Electronic absorption spectra of some substituted indoles. Spectrochimica Acta Part A: Molecular Spectroscopy. 1989. 45(3): 381-389.

[82] Yip, P. Nanometrology using Time-Resolved Fluorescence Techniques. 2016. Ph.D. thesis.

[83] Jung, J. Enhancing Room Temperature Phosphorescence from Organic Molecules by Internal Heavy Atom Effect and External Agents. 2018. Ph.D. thesis.

[84] Grinvald, A. Steinberg, I. Z. On the analysis of fluorescence decay kinetics by the method of least squares. Analytical Biochemistry. 1974. 59(2): 583-598.

[85] Badea, M. G., Brand, L. Time-resolved fluorescence measurements. Methods Enzymol. 1979. 61: 378-425.

[86] Ware, W. R., Doemeny, L. J., Nemzek, T. L. Deconvolution of fluorescence and phosphorescence decay curves. Least-squares method. J. Phys. Chem. 77(17): 2038-2048.

[87] Tatischeff, I., Klein, R. Influence of the environment on the excitation wavelength dependence of the fluorescence quantum yield of indole. 1975. Photochemistry and Photobiology. 22: 221-229.

[88] Aaron, J., Tine, A., Villiers, C., Parkanyi, C., Bouin, D. Electronic absorption and fluorescence spectra of indole derivatives. Quantitative treatment of the substituted effects and a theoretical study. 1982. Croatica Chemica ACTA. CCACAA. 56(2) 157-168.

[89] Charmolue, H. and Rousseau, R. W. L-Serine Obtained by Methanol Addition Crystallization. 1991. AIChE Journal. 37(8).

Note: Passages in this thesis have been quoted verbatim from the following sources:

- Gryczynski, Z., Kimball, J., Fudala, R., Chavez, J., Ceresa, L., Szabelski, M., Borejdo, J., Gryczynski, I. Photophysical Properties of 2-Phenylindole in Poly (vinyl alcohol) Film at Room Temperature. Enhanced Phosphorescence Anisotropy with Direct Triplet State Excitation. Methods Appl Fluoresc. 2020. 8(1):014008.

- Chavez, J., Ceresa, L., Kitchner, E., Kimball, J., Shtoyko, T., Fudala, R., Borejdo, J., Gryczynski, Z., Gryczynski, I. On the possibility of direct triplet state excitation of indole. JPPB:Biology. 2020. 208.

- Chavez, J., Kimball, J., Ceresa, L., Kitchner, E., Shtoyko, T., Fudala, R., Borejdo, J., Gryczynski, Z., Gryczynski, I. Luminescence properties of 5-Bromoindole in PVA films at room temperature: Direct triplet state excitation. Journal of Luminescence. 2021. 230.

- Chavez, J. L., Ceresa, L., Reeks, J. M., Strzhemechney, Y., Kimball, J., Kitchner, E., Gryczynski, Z., Gryczynski, I. Direct Excitation of Tryptophan Phosphorescence. A New Method for Triplet States Investigation. Methods Appl. Fluoresc. 2022.

- Kitchner, E., Seung, M., Chavez, J., Ceresa, L. Kimball, J., Gryczynski, Z., Gryczynski, I. The Role of Observation Conditions in Fluorescence Measurements: Importance of G-factor correction, Magic Angle and Observation Wavelengths. Methods Appl. Fluoresc.

All Figures were reprinted with permission from Methods in Applications in fluorescence, JPPB:Biology, and Journal of Luminescence.

VITA

Personal Background	Jose Luis Chavez Fort Worth, Texas Son of Jose Luis Chavez and Maria Antonia Chavez	
Education	Doctor of Philosophy Department of Physics & Astronomy Texas Christian University Fort Worth, Texas, USA	2022
	Master of Arts Department of Physics & Astronomy Texas Christian University Fort Worth, Texas, USA	2018
	Bachelor of Science Department of Physics University of Texas at Arlington Arlington, Texas, USA	2015
	Associates of Arts Tarrant County College Fort Worth, Texas, USA	2013
	Diploma – Southwest High School Fort Worth, Texas, USA	2010
Experiences	Teaching Assistantship, Texas Christian University 2017-2021 Cosmic Origins, Physics I & II (calc & algebra) Fort Worth, Texas, USA	
	Research Assistantship, Texas Christian University 2017-2021 Time Resolved Fluorescence Spectroscopy Lab Advisor: Dr. Zygmunt Gryczynski	
	Student Research Volunteer, UNT Health Science Center 2017-2020 Center for Fluorescence Technologies and Nanomedicine Advisor: Dr. Zygmunt Gryczynksi	
	Undergraduate Research, University of Texas at Arlington 2013-2015 Department of Physics Advisor: Dr. Wei Chen	

Abstract

DIRECT TRIPLET STATE EXCITATION OF INDOLE DERIVATIVES: NOVEL

APPLICATIONS OF PHOSPHORESCENCE

By Jose Luis Chavez, 2022

Department of Physics and Astronomy

Texas Christian University

Thesis advisor: Dr. Zygmunt "Karol" Gryczynski

Photophysics is by definition the study of the interaction of light and matter. When this interaction takes places, molecules can absorb light and release a photon of certain energy. This is called photoluminescence. Photoluminescence can be separated into two emission processes: fluorescence (which happens on the time scale of nanoseconds) from the singlet state and phosphorescence (which happens in the scale of microseconds – seconds) from the triplet state. Phosphorescence emission is several orders of magnitude weaker than fluorescence emission because there needs to be a so-called "forbidden" process- singlet to triplet intersystem crossing- to achieve phosphorescence emission. Indole is an aromatic organic compound which has photoluminescence properties. It also is the side chain in the essential amino acid tryptophan. There have been efforts to use the spectroscopic properties of tryptophan to study proteins and protein interactions since the 1950's. However, most of the work has been done using fluorescence because phosphorescence is much weaker. In this study we propose a new method of achieving phosphorescence emission: direct triplet excitation. Instead of populating the singlet state first and then having intersystem crossing to the triplet state, if one uses longer wavelength (redder) excitation, only the triplet state is populated. This allows us to use the long timescale

(microseconds-seconds) and high anisotropy of phosphorescence to study protein dynamics of much larger biomolecular systems.

I investigated tryptophan's phosphorescence as well as the indole and indole derivatives, 2-Phenylindole and 5-Bromoindole in poly (vinyl alcohol) film. The indole derivatives were chosen to enhance the probability of exciting tryptophan directly to the triplet state.